Chapter 6

Airborne Geophysical Result and Interpretation

6.1 Aeromagnetic result

In this thesis all airborne magnetic results are displayed as digital image maps. They are total magnetic intensity map, residual magnetic intensity map, reduction to the pole map, analytic signal map, vertical derivative map, directional cosine filter map and upward continuation map. Many more images were generated during this study, such as texture filtering, but are not presented in this thesis.

The total magnetic intensity (TMI) map (Fig. 6.1) shows regional high magnetic intensities in the northern part of the surveyed area, such as in Pak Chom, Chiang Khan, and Nam Som districts, and low intensities in southern part of the Loei study area, as in Maung Loei, Na Duang and Wang Saphung districts. These systematic patterns are difficult to interpret. To make it easier for interpretation, we had to remove the International Geomagnetic Reference Field (IGRF) was removed from the raw TMI data. The result is a residual TMI map (Fig. 6.2) showing the difference in locations of high and low magnetic intensities. The relative residual magnetic map shows a rather complex crustal magnetization pattern. Magnetic intensity level ranges from -820 to 980 nT and a base level of the map is -4.25 nT. Local variations of field intensity exceed 500 nT in the eastern part and diminish to less than 100 nT in the central and northwestern parts.

The IGRF corrected TMI map (Fig. 6.2) exhibits three regional magnetic zones, roughly trending in the north-south direction based on intensity, shape, and pattern contrasting in magnetic responses and features. From the east, there exists the high magnetic intensity zone clearly visible on the enhanced map, such as in Nam Som districts. It is likely that the small narrow band with the highest portion orients in the northwest-southeast direction and is located in the western part of Suwan Khuha district. The most prominent low magnetic intensity is in the central part between Na Duang and Pak Chom districts and tends to continue northward to the Pak Chom district and Lao PDR.

Within this zone, there are series of the elongated and relatively higher magnetic intensities trending in the northwest-southeast direction. Additionally, the boundary between the central zone and the eastern zone is displayed by the fairly sharp magnetic contrast as clearly observed at Ban Bun Tan and Ban Khok in Suwan Khuha district. To the west, the zone is characterized by groups of strong, positive, roughly circular anomalies (approximately 2 km in diameter) located in the southern part as seen in areas around Maung Loei and Wang Saphung districts whereas in the north it is represented by the large circular features with the average diameter of about 10 km at Ban That in Chiang Khan district.

Both RTP (Fig. 6.3) and analytic signal (Fig 6.4) maps display similar magnetic features, but more significant, to those of the residual magnetic intensity map. Such enhancements lead to the more outstanding magnetic boundaries. Three magnetic zones as well as geological lithologies and structures shown in the residual magnetic map are quite more distinct in the RTP and the analytic signal maps. In the eastern zone, the intensities usually range from 100 to 400 nT. In the western zone, the intensities vary considerably from 50 to 200 nT. Relatively low magnetic intensities from 0 to 50 nT are clearly observed in the central zone from Pak Chom To Na Duang districts. The RTP map shows the highest magnetic intensity in the eastern zone with the average peak to peak at about 700 nT. These high anomalies are oriented in the north-south trend with the total length of about 40 km from Ban Bun Tan to Phu Sang Yai. The western edge of this anomaly is marked by a sharp magnetic gradient in the northwest-southeast trend extending from Suwan Khuha to Nam Som districts in Nong Bua Lumphu province. In the western zone, the relatively low magnetic intensity in area east of Tha Li district is also distinct. The analytic signal image shows the marked narrow zone between the eastern and central parts better than those of the previously described images. However, there exist some sparely distributed narrow zones, immediately south of Pak Chom which show rather high magnetic intensities. It should be emphasized that the boundary contrast within individual zones are quite clear.

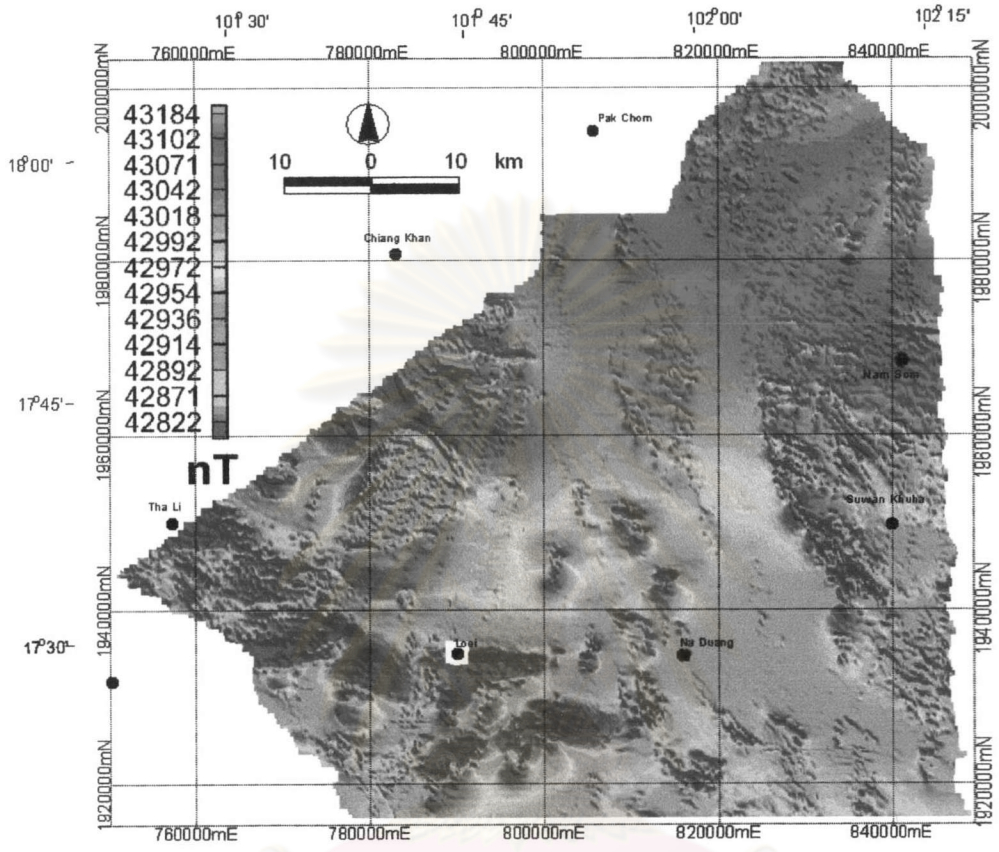

Figure 6.1 Aeromagnetic survey map of the Loei area showing TMI grid image, with grid cell of 200m.

ศูนย์วิทยทรัพยากร
จุฬาลงกรณ์มหาวิทยาลัย

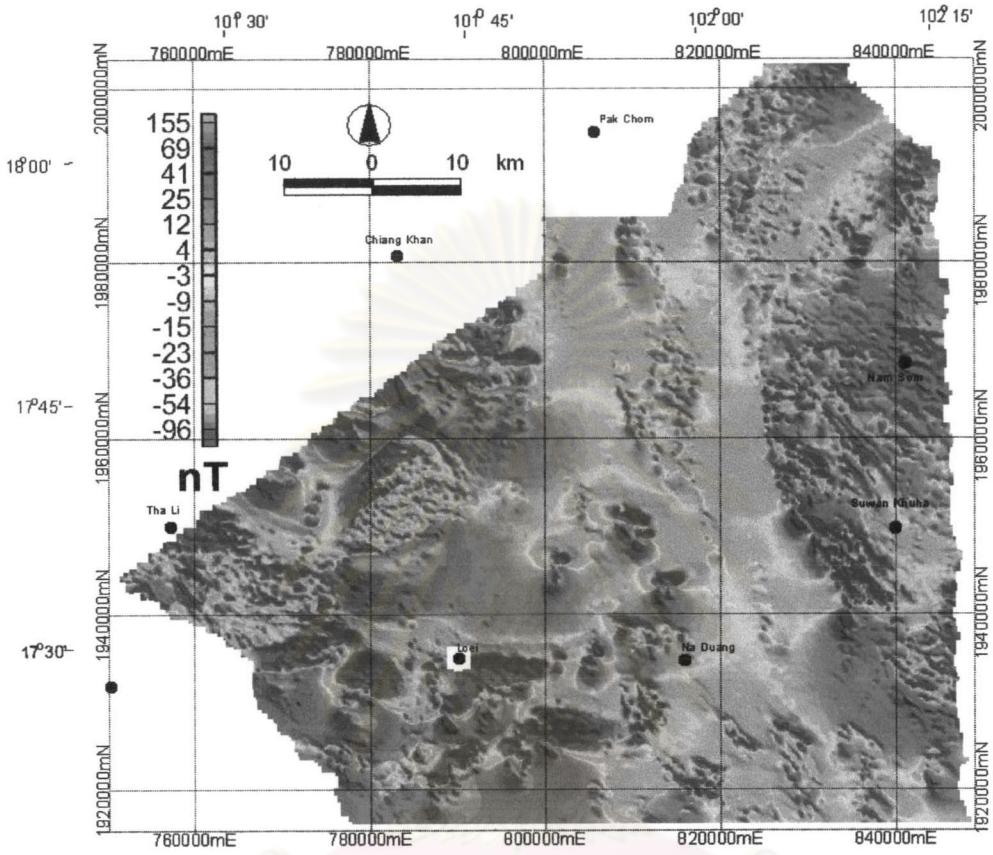

Figure 6.2 Aeromagnetic survey map of the Loei area showing TMI grid after removal of IGRF.

ศูนย์วิทยทรัพยากร
จุฬาลงกรณ์มหาวิทยาลัย

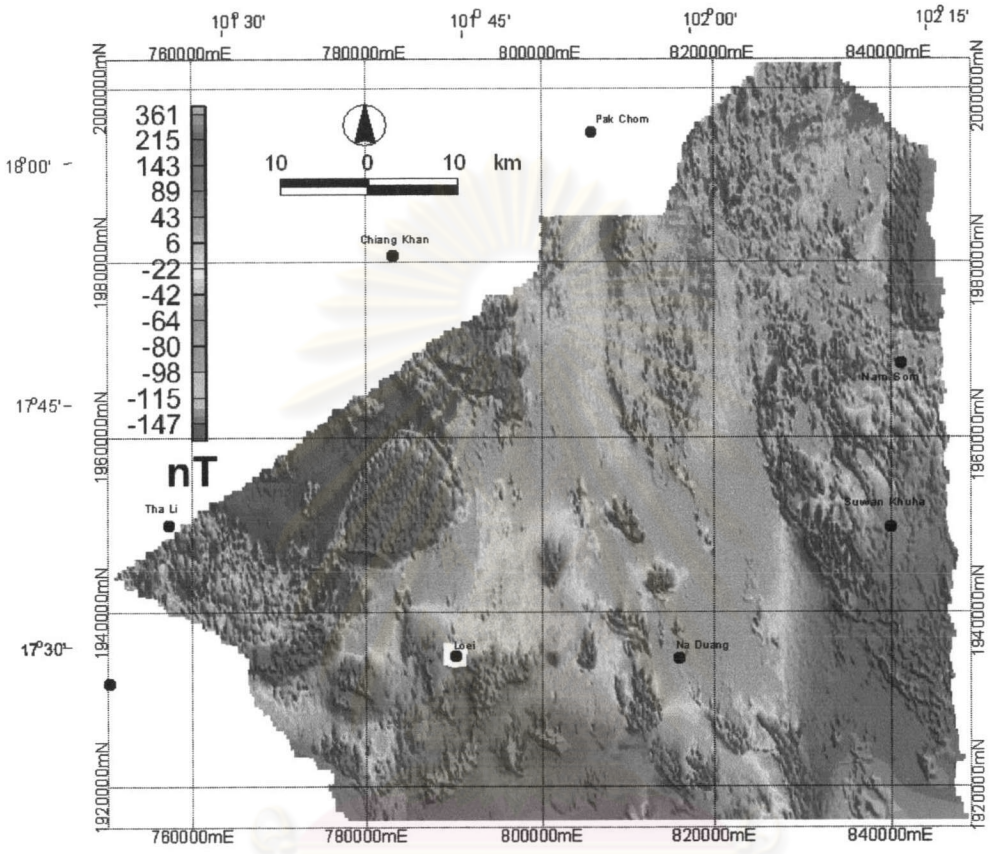

Figure 6.3 Aeromagnetic survey map of the Loei area showing reduction to the pole (RTP) image using the second inclination (I') 30° .

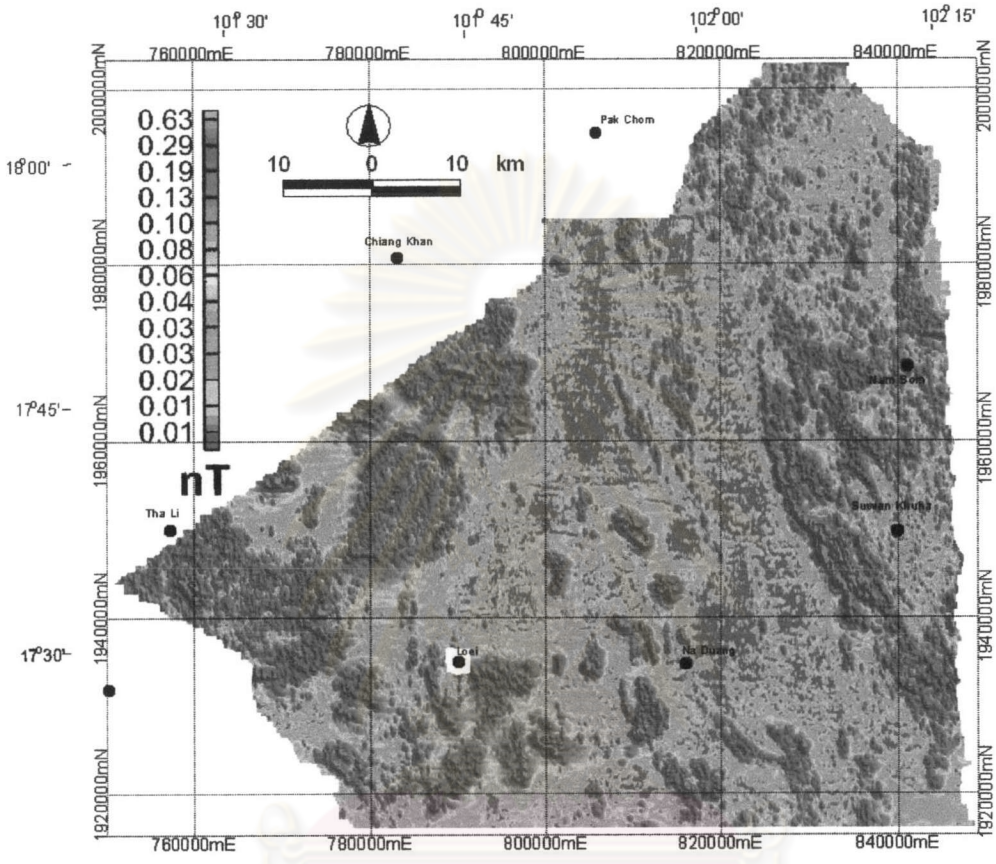

Figure 6.4 Aeromagnetic survey map of the Loei area showing analytic signal image of total magnetic intensity.

ศูนย์วิทยทรัพยากร
จุฬาลงกรณ์มหาวิทยาลัย

Two kinds of derivative maps are applied in this paper. They are the first vertical derivative (Fig. 6.5) and the second derivative (Fig. 6.6) maps following RTP filtering. By applying automatic gain control, both derivative maps reveal significant magnetic patterns such as linear structures or lineaments. The unit or zone boundaries are quite clear when using the first vertical derivative (Fig. 6.5). Major folded structures in the central zone and a large intrusion body are distinct. As shown in Fig. 6.5, it is quite clear that linear patterns are more prominent in the east than those in the central and western parts, and most of the northwest lineaments are crossed-cut by the northeast lineaments. Good examples are at Ban Huai Na, Pak Chom district and Ban Nam Song, Nam Som district. Though anomalies of the second derivative map are less clearly defined, this kind of enhanced map cannot display the well-defined boundaries of the eastern, central, and western unit. However, both enhanced maps can illustrate the similar lineament pattern.

The difference in lineament patterns is clear for enhanced magnetic zones as displayed by directional cosine filters. As shown in Fig 6.7, when filter rejection was applied to the total magnetic map, it is observed that the enhanced may displays the prominent lineaments close to the north-south direction. On the other hand, when a pass direction was used for a directional cosine filter in the map, the northwest-southeast lineament (Fig. 6.8) pattern is clearly observed better than those of the other maps and there are few north-south features. Good examples are at Nam Som and Suwan Khuha districts. The continuous lineaments, about 60 km in length, of this direction seem to cross-cut three regional magnetic zones earlier mentioned. Well-defined examples are Muang Loei to Na Duang Districts. Additionally, some lineaments in the southwest of Pak Chom and southeast of Chiang Khan districts show minor displacements, as illustrated in Figs.6.5 and 6.6. The result shown in these maps clearly indicates that most of the northwest-trending lineaments are cross-cut by the northeast lineaments, such as those found in south of Pak Chom district (see Fig.6.5).

The upward continuation maps (Figs. 6.9, 6.10 and 6.11) show the high magnetic anomalies varying in geometry and locations at different depth. Low magnetic

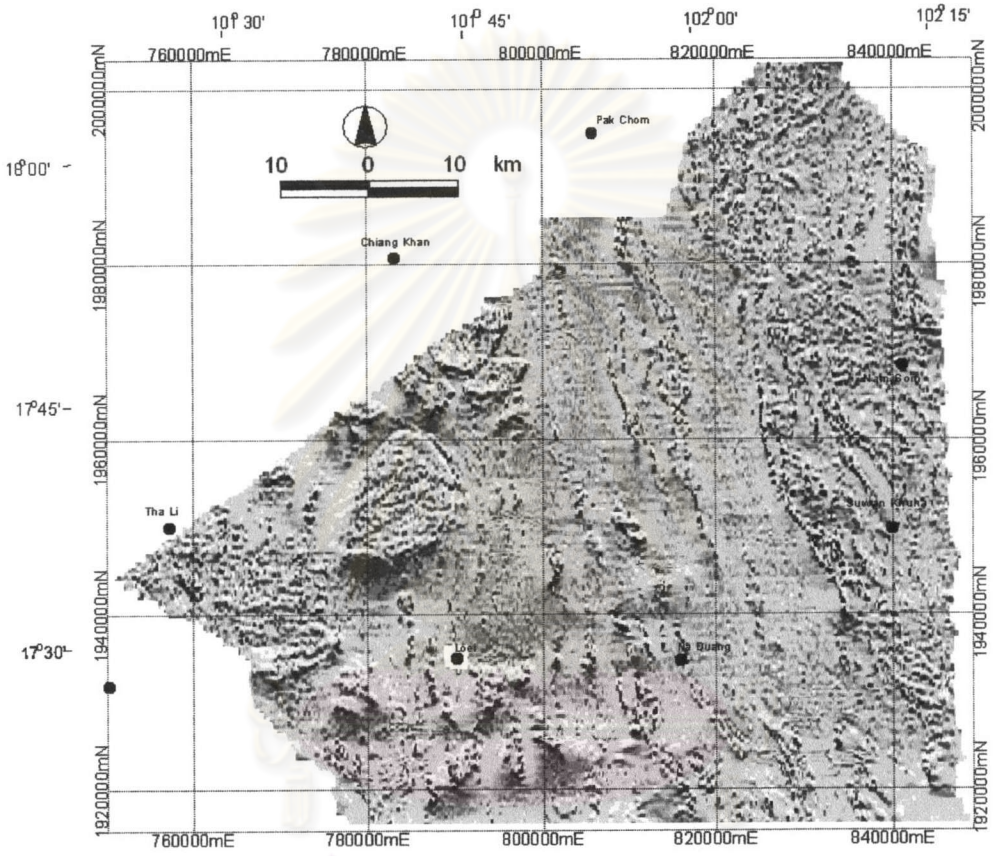

ศูนย์วิทยทรัพยากร
จุฬาลงกรณ์มหาวิทยาลัย

Figure 6.5 Aeromagnetic survey map of the Loei area showing first vertical derivative with automatic gain control image.

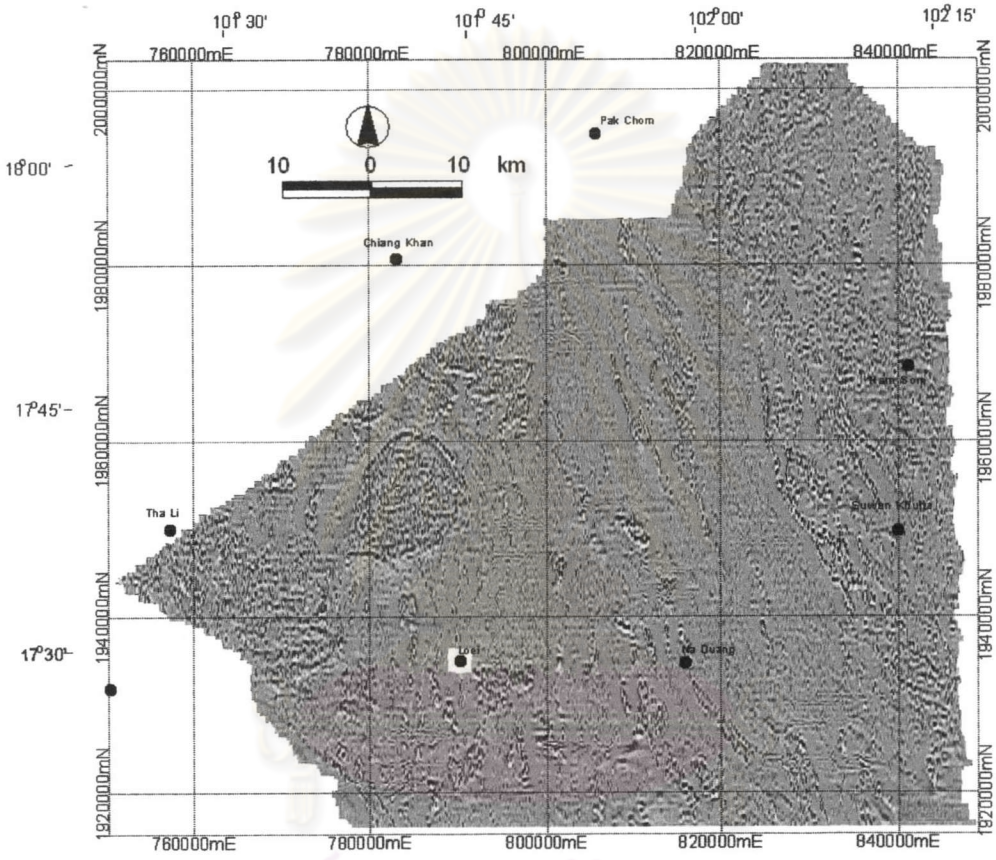

ศูนย์วิทยทรัพยากร
จุฬาลงกรณ์มหาวิทยาลัย

Figure 6.6 Aeromagnetic survey map of the Loei area showing second vertical derivative with automatic gain control image.

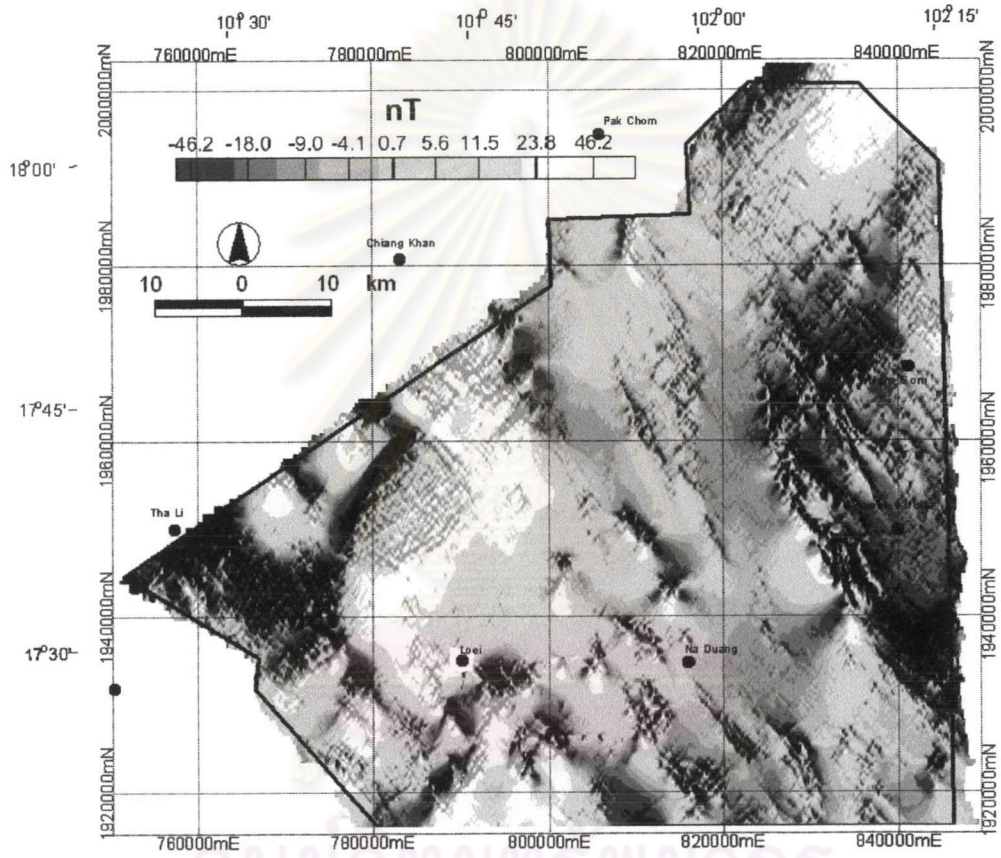

ศูนย์วิทยทรัพยากร
จุฬาลงกรณ์มหาวิทยาลัย

Figure 6.7 Aeromagnetic survey map of the Loei area showing total magnetic intensity map with directional cosine filter allowing a north-south direction.

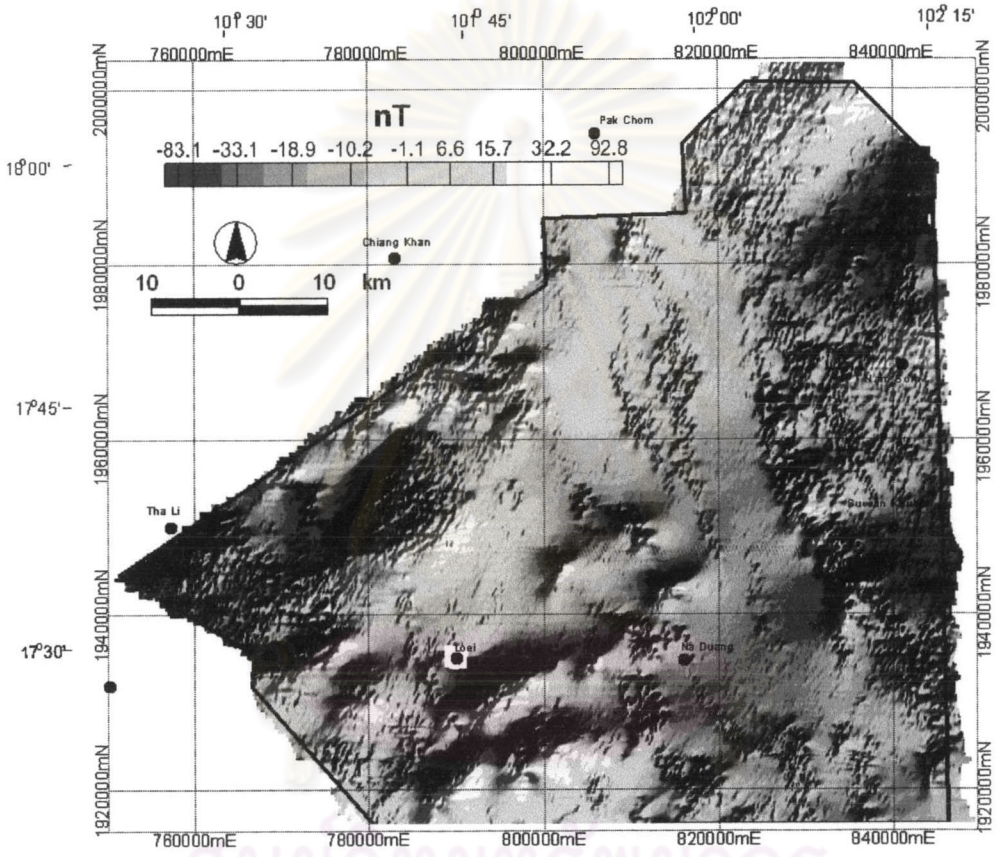

ศูนย์วิทยทรัพยากร
จุฬาลงกรณ์มหาวิทยาลัย

Figure 6.8 Aeromagnetic survey map of the Loei area showing total magnetic intensity map with directional cosine filter a northwest-southeast direction using pass direction.

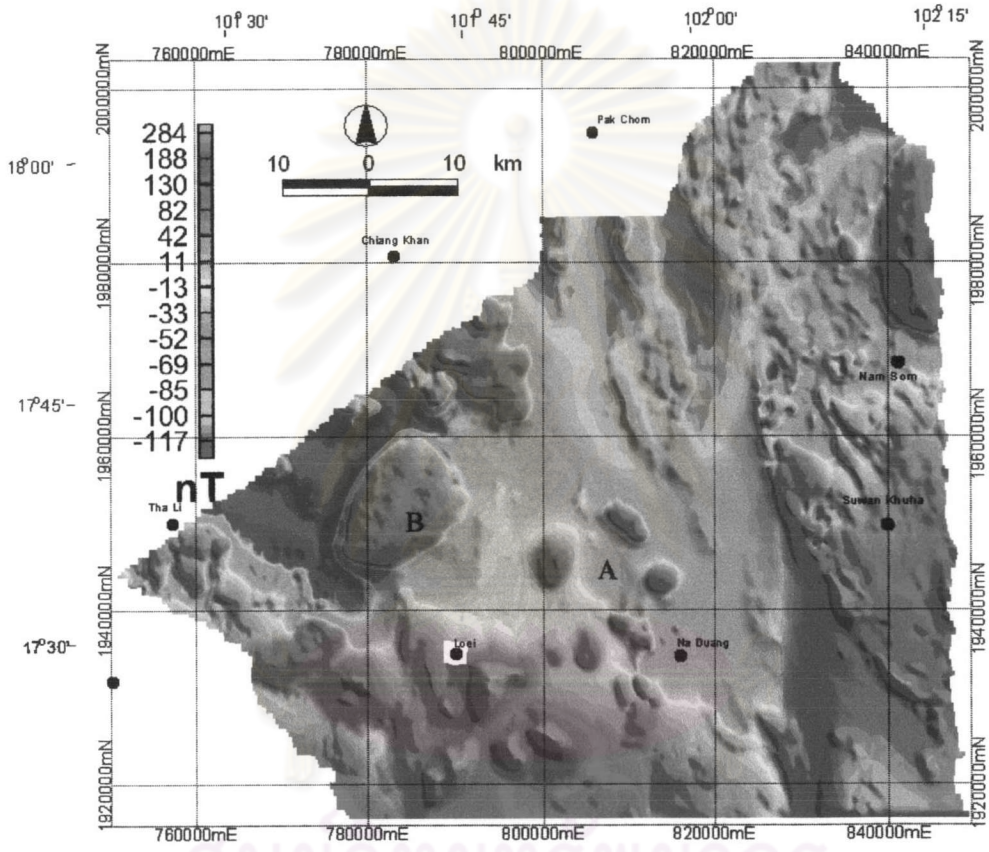

ศูนย์วิทยทรัพยากร
จุฬาลงกรณ์มหาวิทยาลัย

Figure 6.9 Aeromagnetic survey map of the Loei area showing upward continuation images using the different distance from the ground level 500 m.

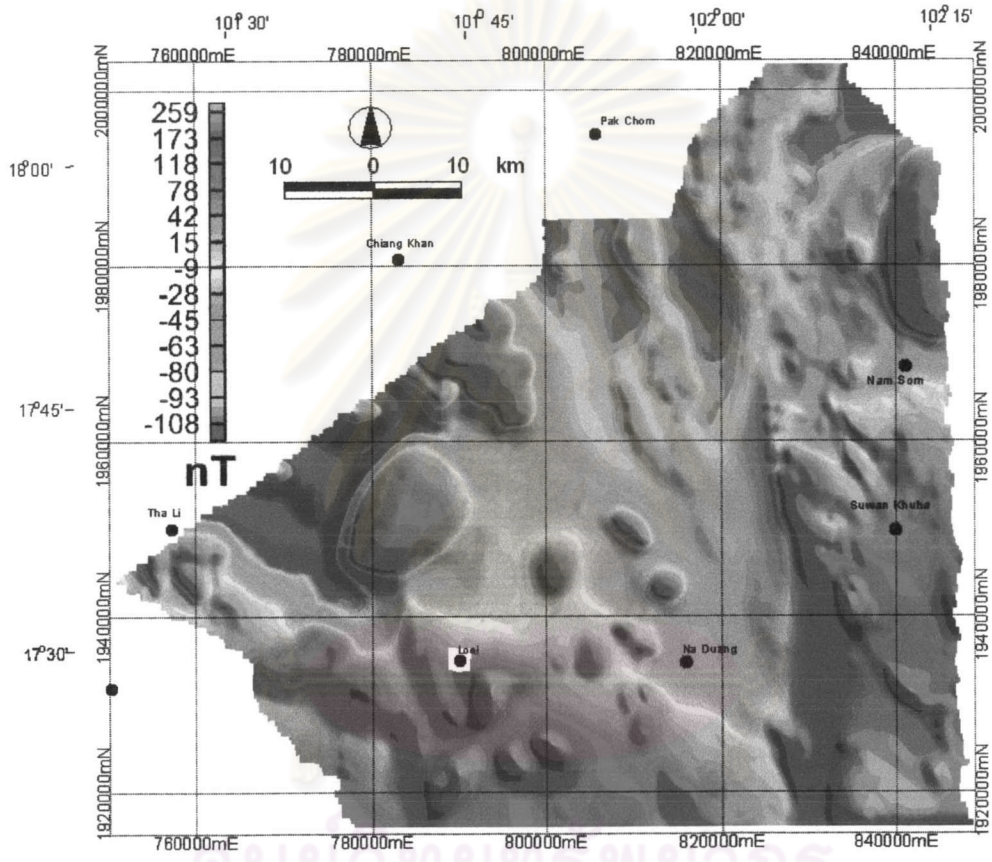

ศูนย์วิทยทรัพยากร
จุฬาลงกรณ์มหาวิทยาลัย

Figure 6.10 Aeromagnetic survey map of the Loei area showing upward continuation images using the different distance from the ground level 1,000 m.

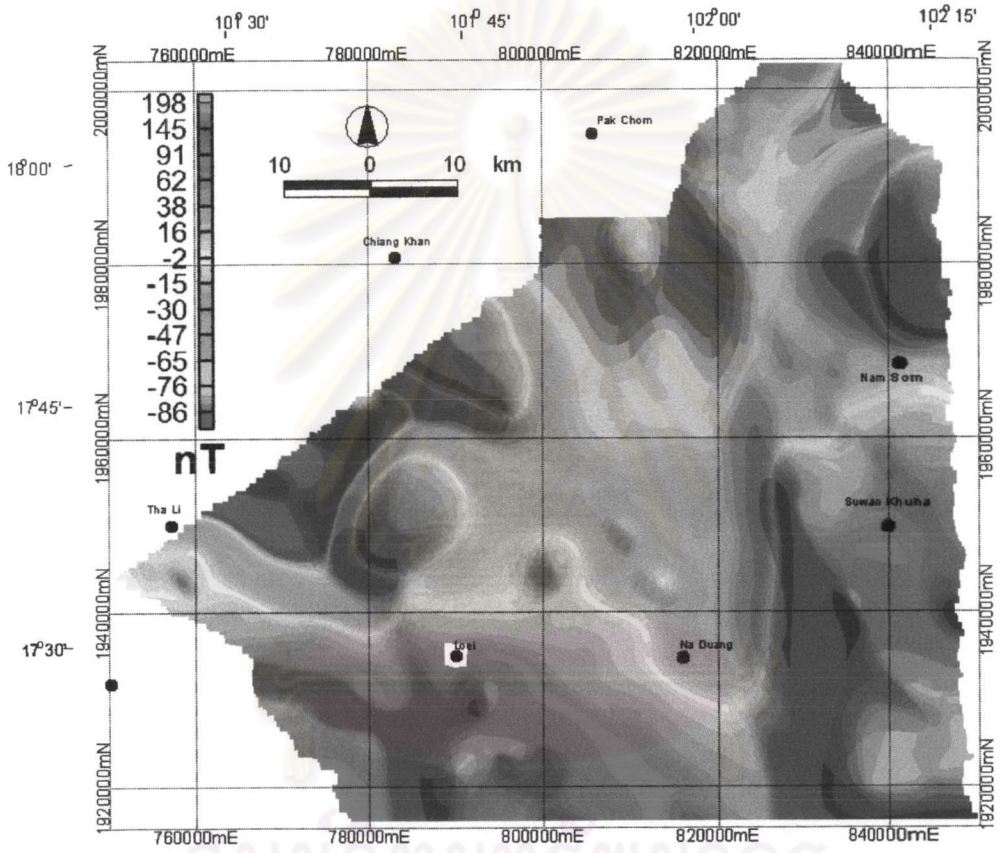

ศูนย์วิทยทรัพยากร
จุฬาลงกรณ์มหาวิทยาลัย

Figure 6.11 Aeromagnetic survey map of the Loei area showing upward continuation images using the different distance from the ground level 3,000 m.

anomalies are found only in the northern part of the study area, such as east of Tha Li and south of Pak Chom districts. Three unit boundaries can be observed well from the RTP map (Fig. 6.3). However the folded structure in areas between Wang Saphung and Na Duang are less clear, and much obliterated fairly when using upward continuation from the depths of 500 m (Fig. 6.9), 1,000 m (Fig. 6.10), and 3,000 m (Fig. 6.11). This loss of short wavelength content is to be expected. Additionally, the folded structures to the south of the Pak Chom area are not clear when applying upward continuation from the depths of 1,000 m and 3,000 m. However, it is interesting that the low anomalous values are also shown at the east of Tha Li even from the depth of 3,000 m. For example, groups of circular features in the central part (A in Fig 6.9) are changed to the small circular magnetic body in the deeper part, whereas the large circular magnetic body (B in Fig. 6.9) in the western part remains similar in sizes and shape continuity at depth of at least 1 km.

6.2 Comparison with other results

In order to interpret geophysical data more reliable and more accurately, in this study we integrated the processed aeromagnetic data with the other data. They are electromagnetic, radiometric, gravity, Landsat and digital elevation data.

6.2.1 Airborne electromagnetic (AEM) result

Airborne electromagnetic data (AEM) have proved complementary to magnetic data in terrains, enabling more precise location and redefinition of the geological structures which no significant anomalies in aeromagnetic data. In this study, the AEM data are presented as digital image maps. Good samples of data processing using the ER Mapper are shown in Fig 6.12 and 6.13, respectively, applying 912 Hz of the inphase and quadrature components to AEM data. The red color represents the high conductor, which mostly corresponds to the weak zone, consisting of water and clay and area of rivers and streams in a valley. This image is useful for identifying the continuous faults that are not shown in aeromagnetic data.

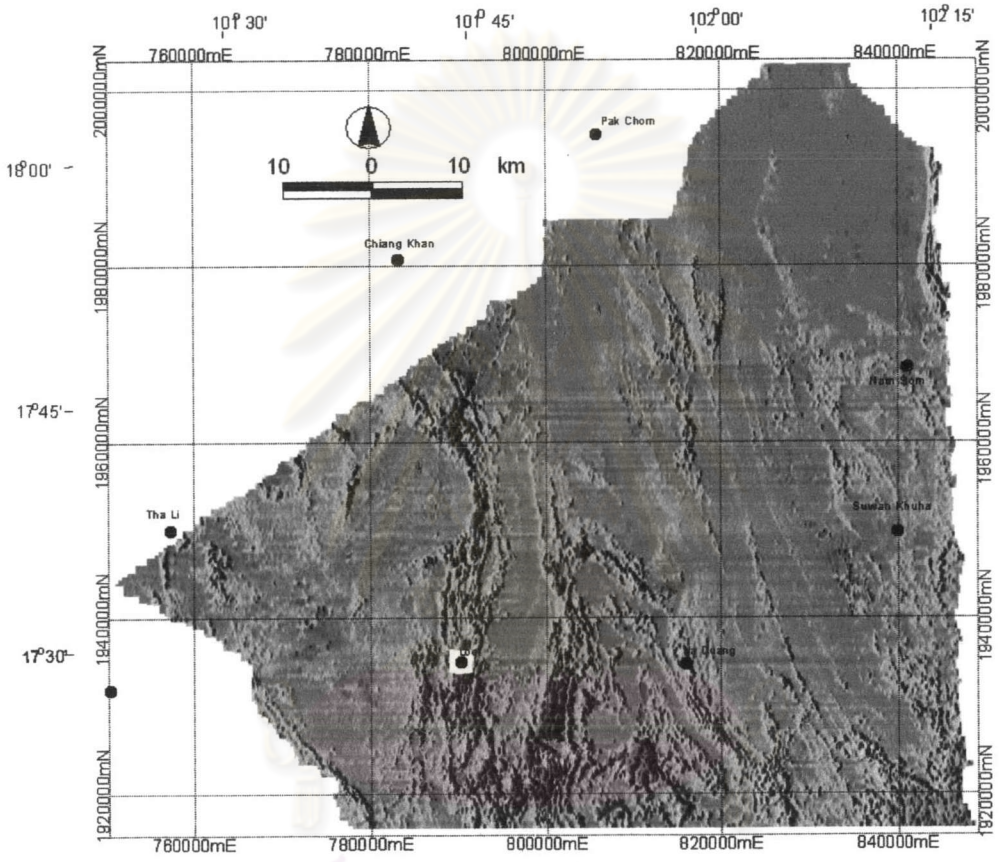

Figure 6.12 Airborne electromagnetic survey map of the Loei area showing inphase component responses at 912 Hz in coplanar configuration.

ศูนย์วิทยทรัพยากร
จุฬาลงกรณ์มหาวิทยาลัย

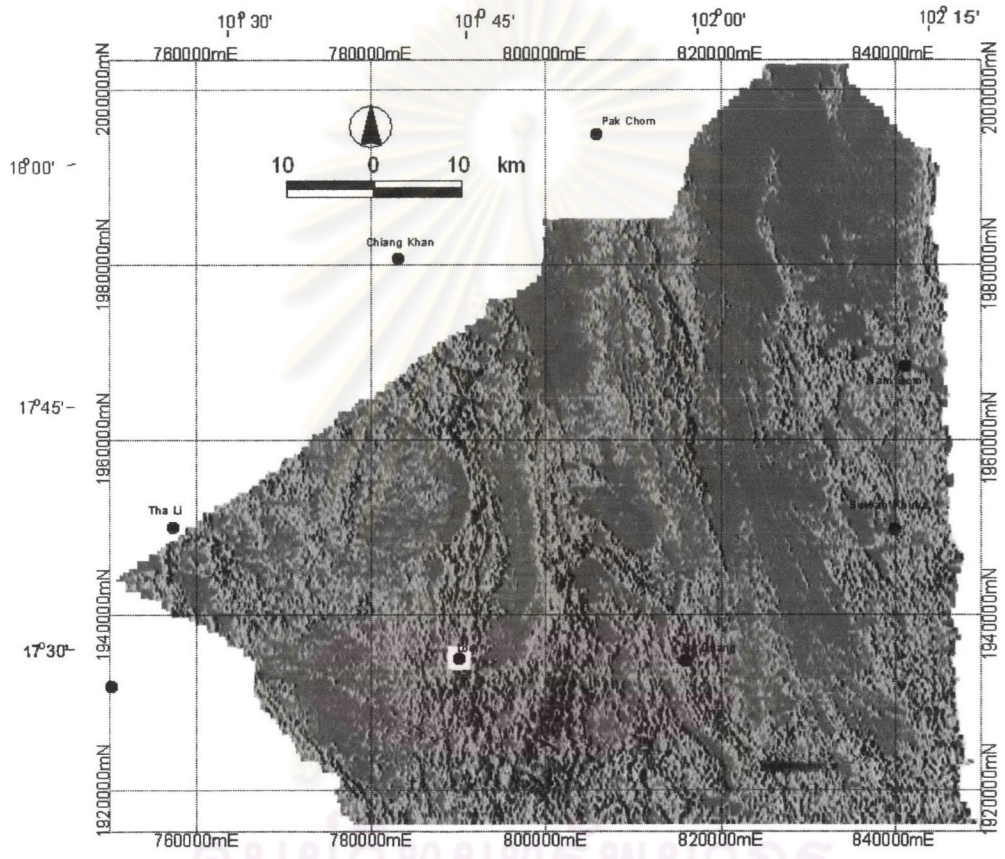

Figure 6.13 Airborne electromagnetic survey map of the Loei area showing quadrature component responses at 912 Hz in coplanar configuration.

ศูนย์วิทยทรัพยากร
จุฬาลงกรณ์มหาวิทยาลัย

Conductivity along fault zones is believed to be caused by strongly weathered bedrocks to clay and/or graphite formed along fault zones.

In Fig. 6.12, the folded structures can be observed quite well, particularly those in the southern part of the study area between Maung Loei and Na Duang. Moreover, the zone boundaries in the eastern, central, and western parts can also be easily visualized, corresponding with these of the processed RTP map. Additionally, the result also indicates that the boundary between western and central zones of the Loei study area become more obvious than those of the RTP data. Amplitude of inphase and quadrature values at the same location always indicate conductive bodies. For most of EM data in this area, quadrature values are generally more useful for interpretation than the inphase values, representing the conductors that correspond with alluvium areas near the river and stream valley. Good examples are at near the Loei river. Some negative linear features, especially in the eastern part, align in the northwest trend as clearly observed at Nam Som and Suwan Khuha districts. High quadrature values particularly in the eastern part are observed at Ban Bun Tan and- Ban Na Klan shows abrupt decreasing values that are inferred as traces of faults in this area. It is believed that differential weathering along bedding planes and clay in river valleys due to the dominant sources for the EM conductor.

Fig. 6.14 shows apparent resistivity complied from the electromagnetic response at the frequency of 4,200 Hz in coplanar configuration. This image is converted to a conductivity image map by multiplying -1 in grid data. This image is displayed using a color scheme with high conductivity area appearing red and low resistive area as blue. Lineaments and boundaries of rock units are clearly defined. This is due to the difference in resistivity contrast, especially, the high resistivity of the sandy soil over the granite intrusions at Ban That and Phu Mon.

The EM results show that the apparent resistivity map created from the enhanced data are extremely valuable for geological mapping and interpretation, and used for checking data integrity, particularly drift problems. Apparent resistivity in each frequency is calculated from responses of inphase and quadrature values.

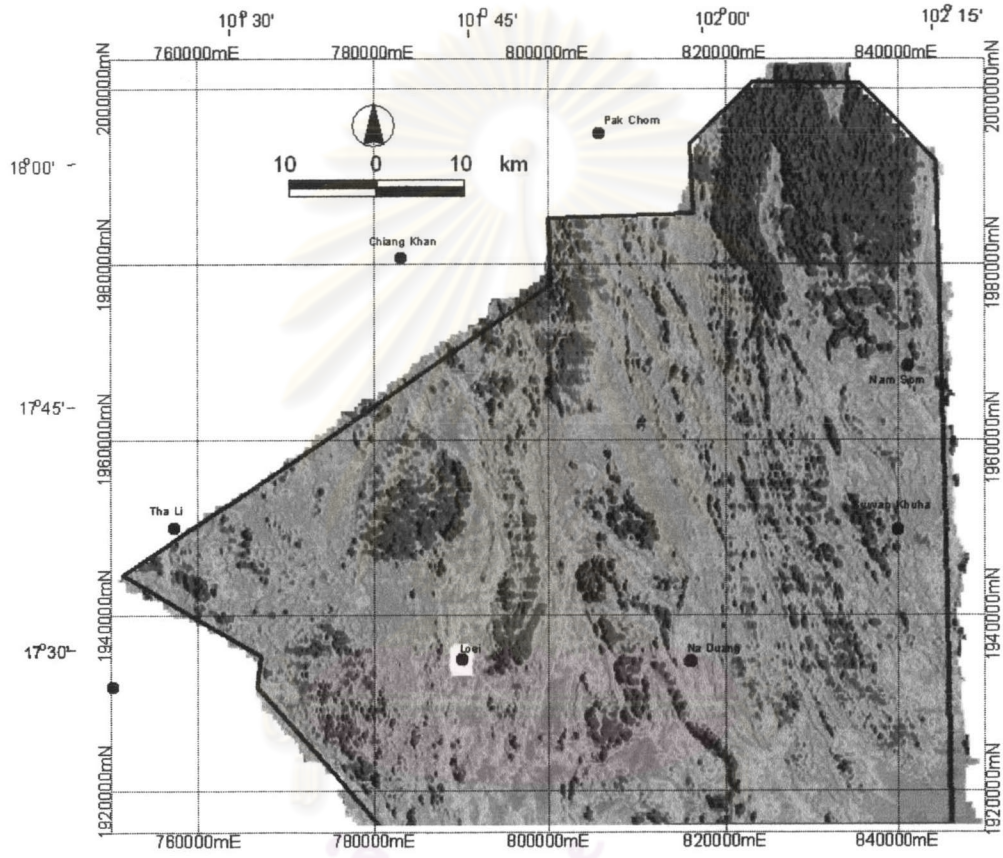

ศูนย์วิทยทรัพยากร
จุฬาลงกรณ์มหาวิทยาลัย

Figure 6.14 Airborne electromagnetic survey map of the Loei area showing apparent conductivity responses at 4,200 Hz in coplanar configuration.

Noise is often a significant issue in AEM data, where signal to noise ratios can be quite low, particularly over resistive terrains. Common noise sources are electromagnetic, vibration, or movement of the EM bird. The two main types of non-geological noises observed are individual spikes and lower amplitude, high-frequency noise. For this study, non-linear filtering and the first vertical derivative filtering is applied in the AEM data to remove the high frequency noise, and to carry out leveling or drift correction, respectively.

6.2.2 Airborne radiometric result

Airborne radiometric data (Fig. 6.15) are shown as a composite color image or a ternary map with combined intensities of potassium (K), throrium (Th), uranium (U) given as intensity of red, green, and blue. The radiometric data have proved valuable in mapping the stratigraphy and structure of magnetic and non-magnetic rock units in outcrop and for recognizing individual phases and zoning within units such as granitoid intrusion on a residual soil. Because radiometric data show only in the earth surface to the depth of about 30 cm. so the interpretation of radiometric data is mainly controlled by the topography of the area.

The ternary radiometric map shows a brownish green and red to black colors indicating the moderate to high K, Th and U. The radiometric responses are, to some extent, corresponding with the surface geological map (Fig. 2.3). Basically, the low concentrations of U, Th, and K radioactive elements are displayed by black colors. It is widely accepted that pattern of low contents of U and Th and high K contents are characterized by red color. Those of the low content of K but high contents of U and Th are characterized by green color. Additionally, those of medium contents of K, Th and U are observed as brownish green color. It is clearly observed that the western part of the Loei study area displays relatively milder colors than the central and eastern parts, suggesting the less complicated geology and structures located south of Tha Li district,

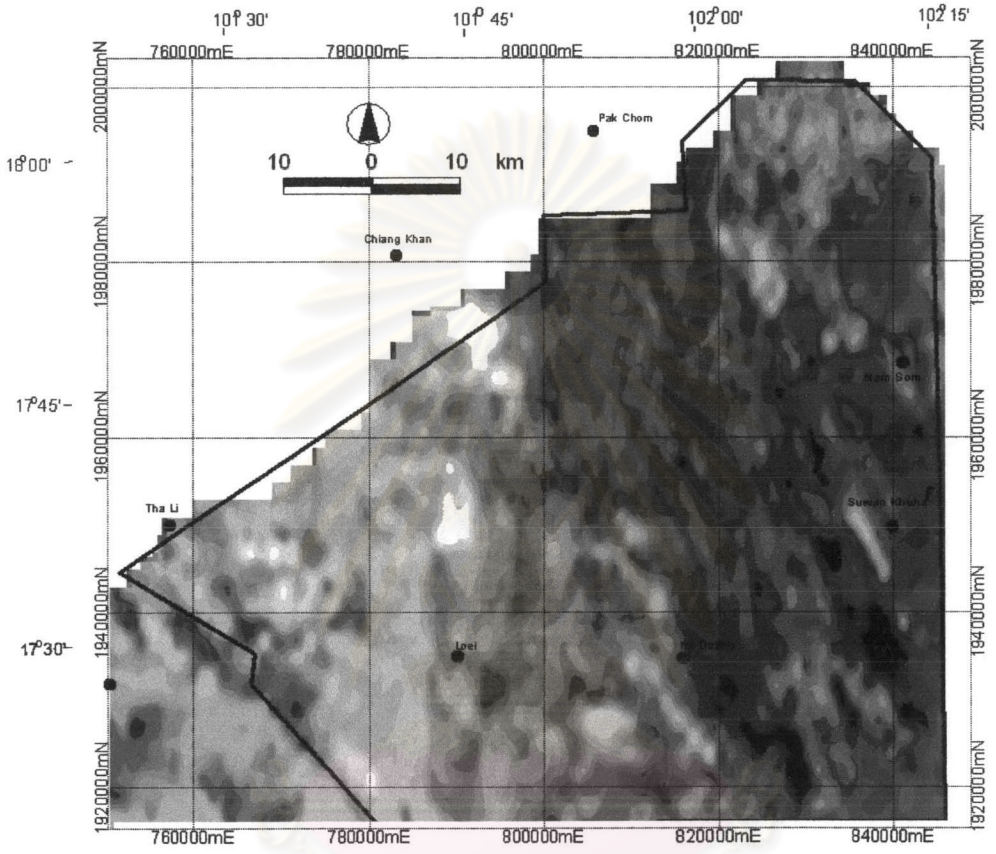

Figure 6.15 Radiometric ternary map from regional survey flown with 1 km line spacing of the Loei study area. White areas are granite out crop and subcrop.

next to the western part of the study area show low radioactive values similar to those of the south central part between Wang Saphung and Na Duang, which is mainly Late Paleozoic rocks. However, unlike the Mesozoic strata, the late Paleozoic strata show "drag " folded structure, suggesting some kinds of subsequent tectonic disturbance. The northwest- trending linear trends in the eastern part suggest the regional structure and also follow the main topography. Similar folded structure found in the western part of the study area in Suwan Khuha district is shown as oval-shaped trend in the ternary map. This may represent the deformational structure in the ultramafic rocks. Such structure, although not clear, can be observed also in the gravity map (Fig. 6.17). It is also interesting that the Late Mesozoic continental red clastic sequences is shown by yellowish to greenish colors, is denoted by relatively linear series trending in the northwest-southeast direction. Such patterns correspond very well with those of the directional cosine filter total magnetic map (see Fig 6.7 and 6.8). In the eastern part such as Ban Pak Chiang and Ban Siang Di, two groups of colors red to brown and violet to pink are presented. These areas are high relief (Fig.6.16), so radiometric responses are equivalent to the original bedrock responses at the surface.

In the northeastern part of the eastern zone, the radiometric responses are represented by the blue color with high U and Th contents, such as at Ban Huai Sai and-Ban Na Yung. These results point to the occurrence of fine grained clastic rocks that correspond with the geological map but are not conformed well to the magnetic response showing the high magnetic intensities of granitic intrusion. The magnetic response suggests the interpreted granitic intrusion underlying the sedimentary rock in this area.

In the southern part of the eastern zone, the responses are distinguished by variable textures. Residual brownish blue-to-blue colors indicate most of high K, and some Th and U contents associated with felsic volcanic rocks and some of sedimentary rocks. The interesting radiometric response in this part is a narrow northwest trend of the low K, Th and U contents shown as slightly black color in the westernmost part of the eastern zone near Ban Bun Tan. This result is corresponded with the high magnetic intensity indicated the characteristic of ultramafic volcanic rocks. Additionally, near this

unit to the east, such as at Ban Khok, is the moderately high K, Th and U contents as displayed by slightly white color. This result may indicate clayey earth on subdued topography between the quartzite ridges formed by weathering of phyllitic and clastic parent materials.

In the central part the brown to red colors indicate sedimentary rocks containing high K concentration. Again this corresponds with the clay derived mostly form weathering shale unit. In the south of this zone, green to blue colors point to areas of high Th and U concentration with associated spots of light brown color. These results correspond with the sedimentary rocks mapped as limestones with some granitic dykes shown in the geological map (see Fig 2.3). In the zone of volcanic basalt, it is characterized by dark blown color indicated the high K and U contents.

The western part shows three different light colors in the ternary map. The radiometric result is represented by light green color indicating high Th as in area of Ban Pak Phu and Ban Na Bon. These areas have fate and low relief topography, so the result indicated silty and sandy sediments of alluvial, deposit cemented or capped by ferruginous material. The high K, Th and U contents show by a circular white color in-Ban That. This surely indicates a granite intrusion covered by thin regolith or thick saporites. The southwestern part, such as in Tha Li district shows a complex of radiometric elements as indicated by green, red and brown colors. This unit is in the high topography, so the radiometric elements are directly implied bedrock, probably volcanic compositions.

ศูนย์วิทยทรัพยากร
จุฬาลงกรณ์มหาวิทยาลัย

6.2.3 DEM result

In this study, essential map of the area used for geological interpretation, particularly for radiometric interpretation is the digital elevation model (DEM,). The DEM map (Fig. 6.16) is displayed as a color shade relief image, a red color indicated the high topography, whereas a blue color represented flat or alluvium area. The DEM is useful to integrate with the radiometric, magnetic and electromagnetic data for mineral prospecting. Moreover, the DEM can be used for identifying the structures such as faults

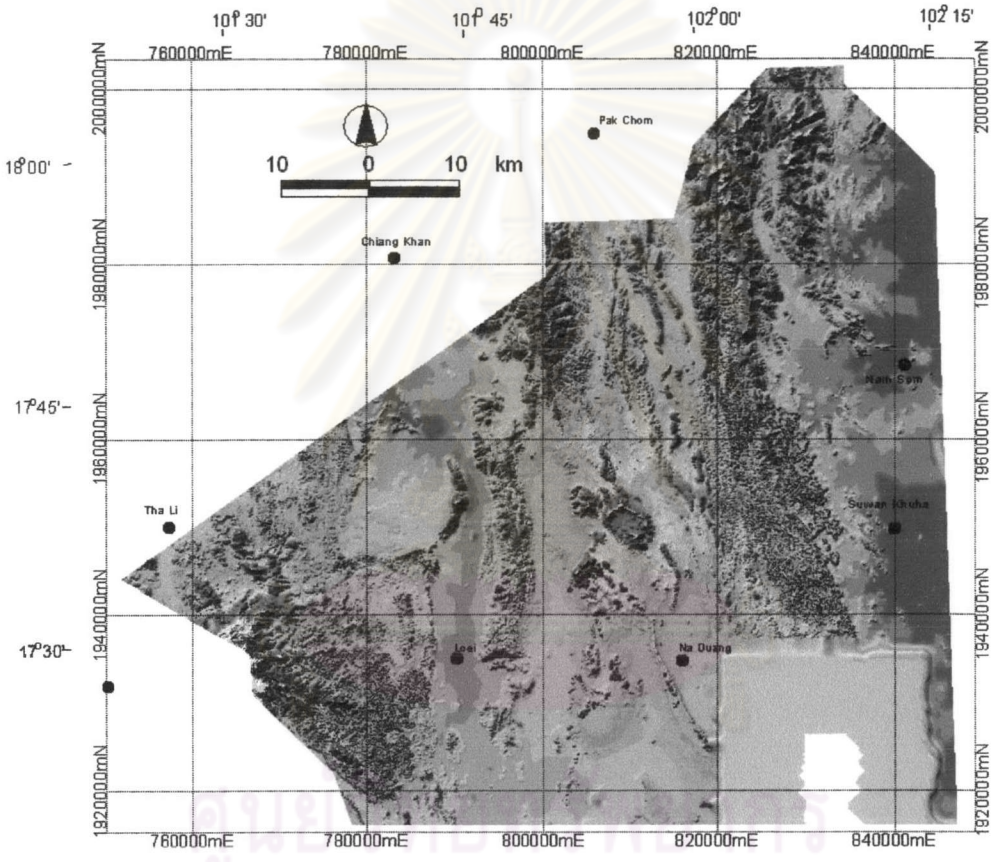

Figure 6.16 Digital elevation map (DEM) of the Loei study area

ศูนย์วิทยทรัพยากร
จุฬาลงกรณ์มหาวิทยาลัย

and folds. Most of high topography areas are in the northern part of the area near Pak Chom and Chiang Khan districts

6.2.4 Gravity result

A total of twelve gravity data points are used to construct the gravity map of the Loei study area. Regional gravity data are commonly used to delineate the position of boundaries at deeper levels than aeromagnetic data. In this study the gravity data are displayed as Bouguer anomaly. Points of measured gravity stations shown on top of grid show low space coverage in the study area (Fig.6.17). This gives so difficult in interpretation and modelling geophysical features, and exiting gravity image not good for tectonic interpretation or explanation at scale of 1:100,000 used in this study.

As shown in Fig. 6.17, the high-density area (red color), such as Suwan Khuha and Nam Som districts, are in the eastern part that may represent the rocks that occurred in the deep crust. On the contrary, the central and the western parts, though display similar characteristics, are quite different in composition from the eastern part. The green to blue colors representing respectively the moderate and gravity values may indicate rocks originating in the much shallower crust.

6.2.5 Remote sensing result

Figure 6.18 shows the Landsat TM5 image of band 7, which was selected by visual examination to study the lineaments. Since the image requested is prepared digitally in the rectangular form, so part of the study area also includes in part of Lao PDR. Thus the usefulness of this map is to describe the continuity of long lineaments extending from NE Thailand to Lao PDR.

As shown in Fig. 6.19 and 6.20, when directional filter using sunlight direction in the northeast and northwest directions was applied to the Landsat TM5 band 7, it is observed that the main structures is shown clearly in the roughly north to north-northwest trend. Three units (east, central, and west) are also divided. This linear feature

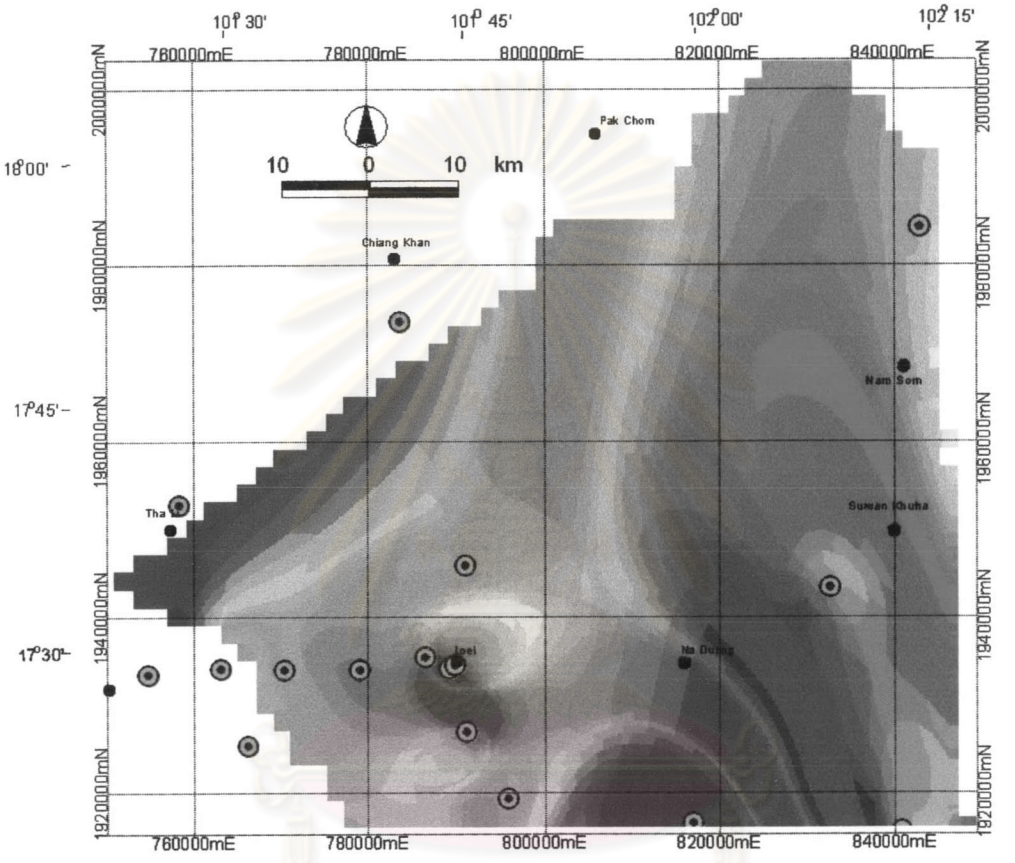

ศูนย์วิทยทรัพยากร
จุฬาลงกรณ์มหาวิทยาลัย

Figure 6.17 Color gravity map of the Loei study area showing stations of gravity measurements (green points).

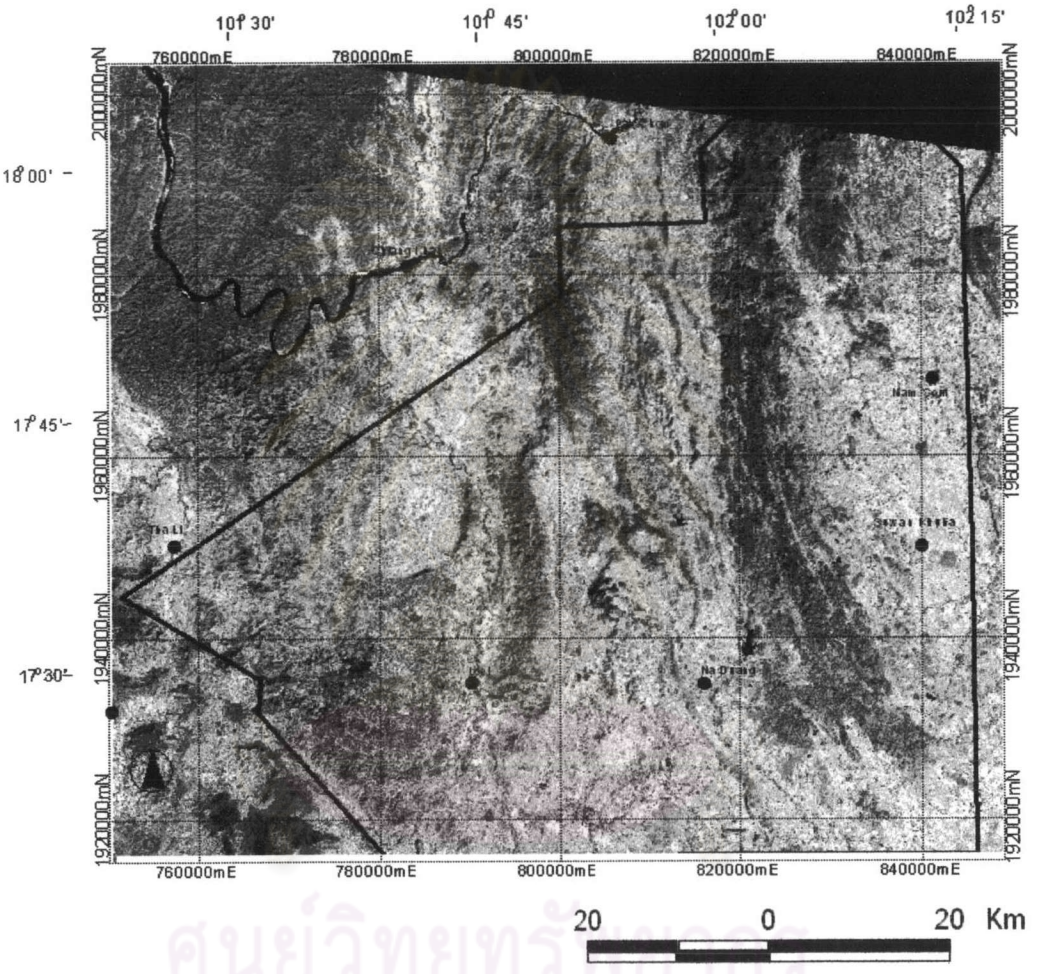

ศูนย์วิทยทรัพยากร
จุฬาลงกรณ์มหาวิทยาลัย

Figure 6.18 Landsat TM5 band 7 image covering the Loei study area.

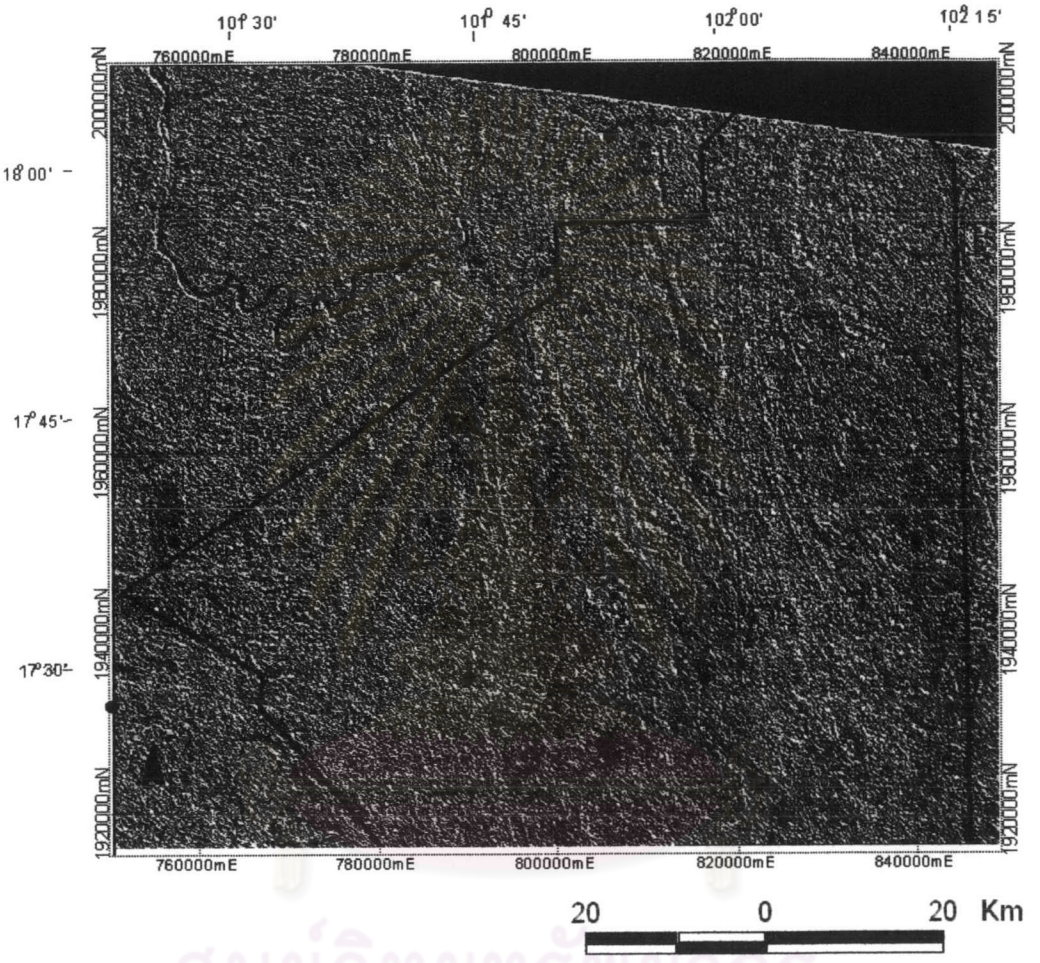

ศูนย์วิทยทรัพยากร
จุฬาลงกรณ์มหาวิทยาลัย

Figure 6.19. Landsat TM 5 band 7 image with enhancement using the directional filter in northeast-southwest direction.

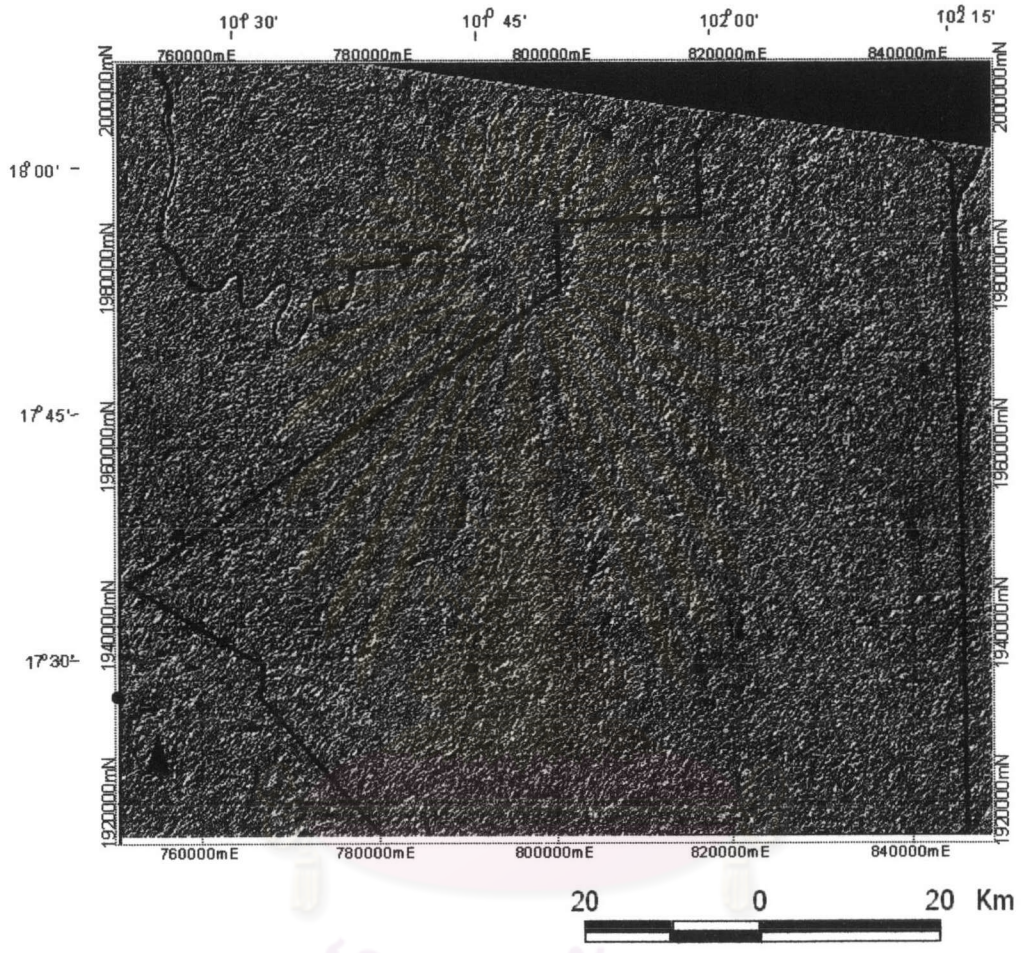

ศูนย์วิทยทรัพยากร
จุฬาลงกรณ์มหาวิทยาลัย

Figure 6.20 Landsat TM 5 band 7 image with enhancement using the directional filter in northwest-southeast direction.

cross-cuts the direction of sunlight, so it was enhanced to get better picture than the original image.

The selection for three TM bands for color display was made using a combination of statistical investigation and visual inspection. In this study two false color composite maps were applied by using compositions of Landsat TM5 band 741 and band 754 combination, respectively, in red, green and blue colors, are shown in Figs. 6.21 and 6.22, respectively.

Color composite of Landsat band 741 shows well-defined forest in high mountain in the north-south direction especially in limestone terranes but the other features are not well observed. Most rock types are shown as purple colors but some areas in southeast part displayed the dark, violet, probably representing the area of magmatic source. Rivers and lakes are shown in black color.

Color composite of Landsat band 754 displays well-defined geology for delineating the continuity of major lineaments. Major northeast-trending lineaments are shown crossing the whole area, especially in the northwestern part. It shows some slip displacement suggesting the strike slip fault. The linear features in the eastern part are also well defined. Tight folds in northwest part, especially in area of Nam Som and Suwan Khuha districts, are crosscut with the northeast lineament. In the central area, such as Phu Phaeng Ma and Phu Khi Theo, the small circular feature near the dark brown color area may indicate the magmatic source or volcanic cone. Most areas are shown in the brownish yellow and some dark brown disseminated areas, particularly in the southern part that may indicate areas of iron rich or volcanic rocks.

The principal component analysis (PCA) is performed using all of the 7 reflected bands of Landsat TM5 data as shown in the Figure 6.23. This image is the principal color composite consisting of red=PC1, green=PC2, and blue=PC3. It shows some degrees

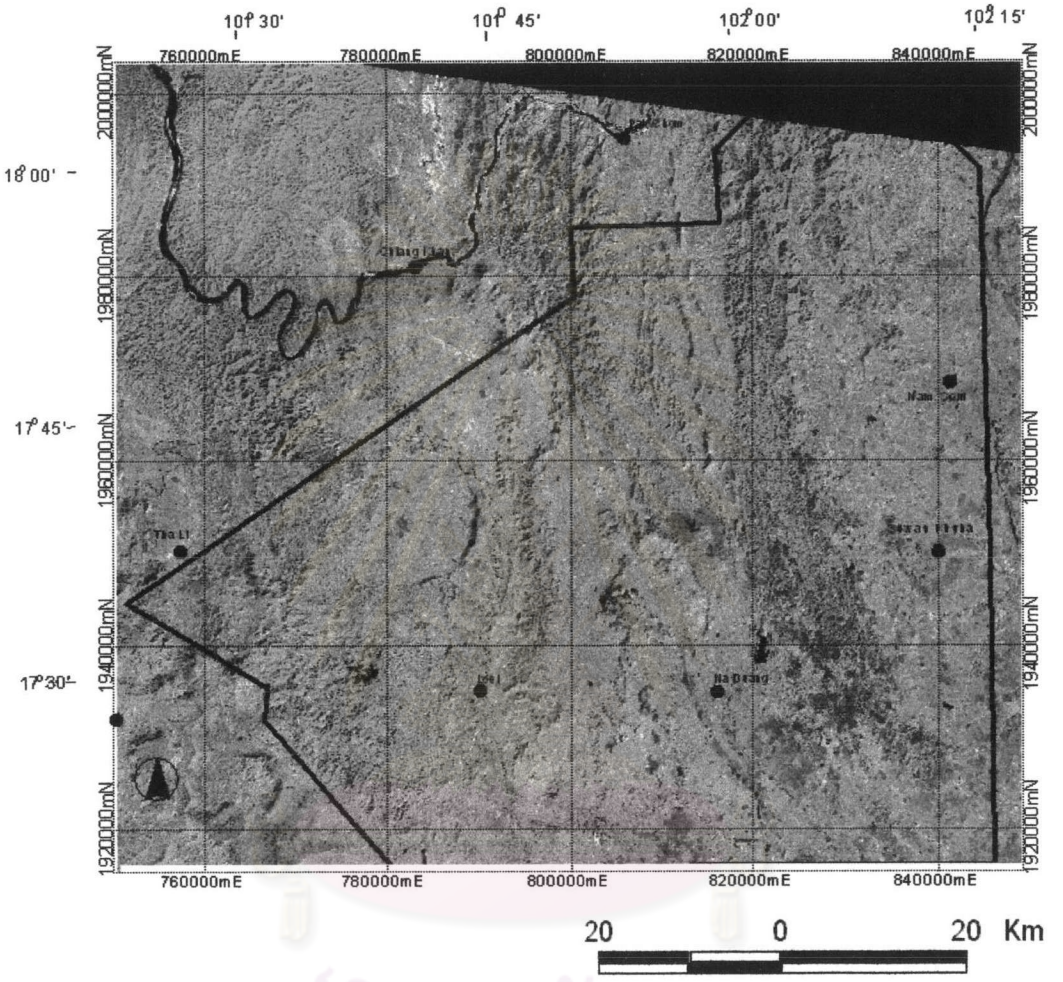

ศูนย์วิทยทรัพยากร
จุฬาลงกรณ์มหาวิทยาลัย

Figure 6.21 False color composite map of Landsat TM 5 band 7, 4, and 1 with red, green and blue, respectively.

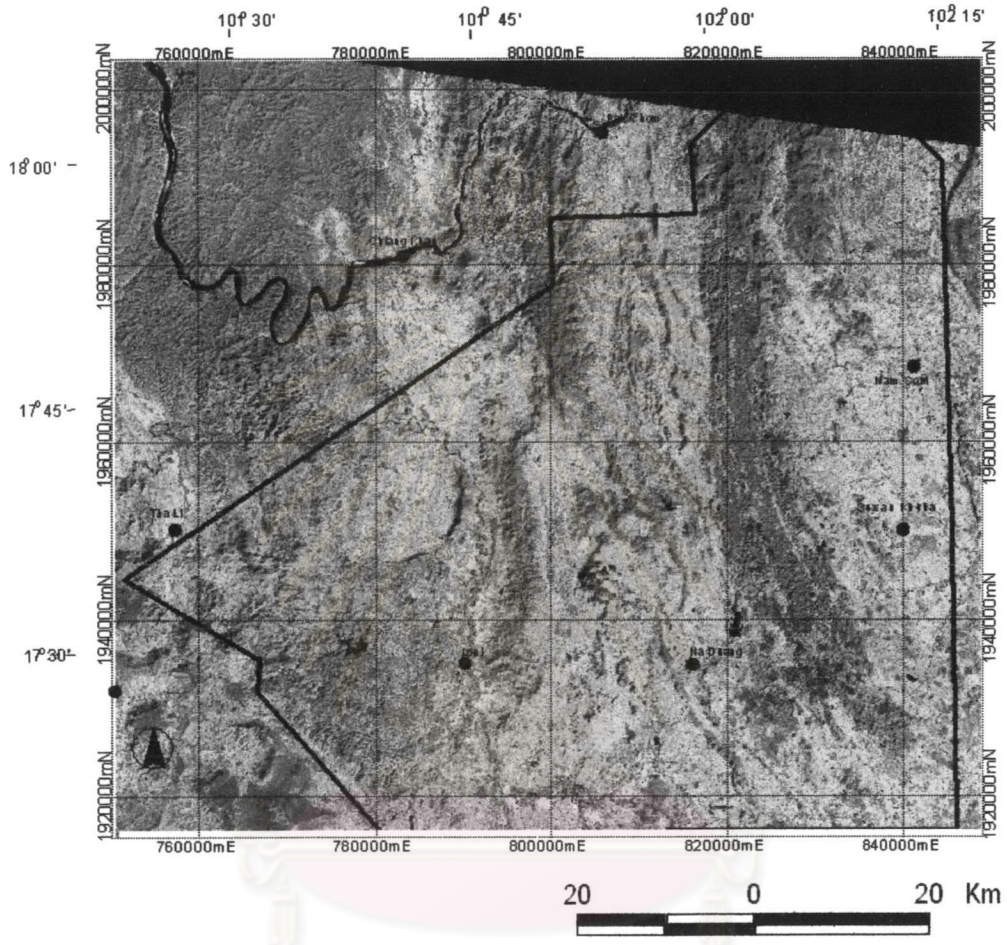

ศูนย์วิทยทรัพยากร
จุฬาลงกรณ์มหาวิทยาลัย

Figure 6.22 False color composite map of Landsat TM 5 band 7, 5, and 4 with red, green and blue, respectively.

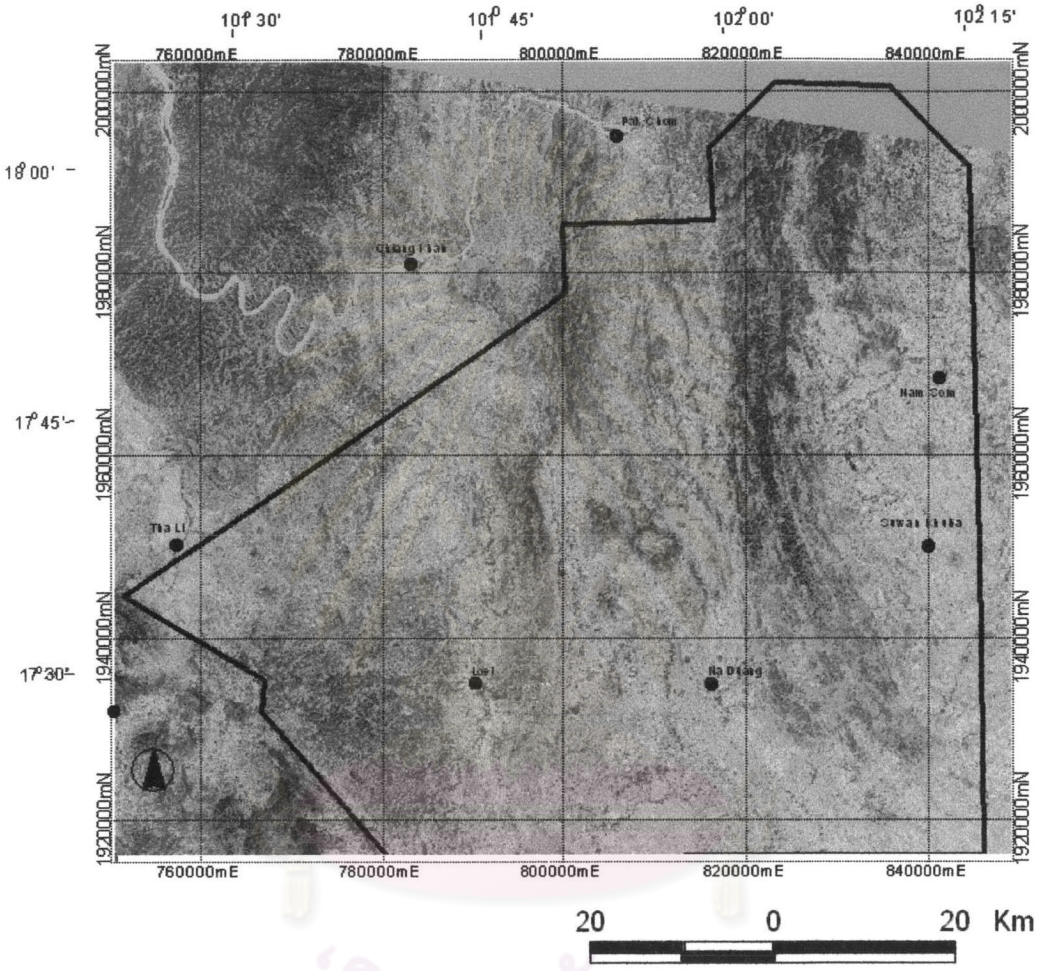

ศูนย์วิทยทรัพยากร
จุฬาลงกรณ์มหาวิทยาลัย

Figure 6.23 Landsat TM 5 after enhancement using principle component analysis (PCA) of the Loei study area.

of discrimination between different lithologies. The western part shows the purple color that possibly indicates andesite and granitic rocks. The metamorphic rocks in the eastern part appear blue-green, which may be covered by forest areas. The limestone is distinct in green color. The small circular features in the central of the area appear in wine purple color. The areas covered by alluvium tend to be yellow, with uncertain boundaries.

6.2.6 Magnetic susceptibility result

A rock-sampling program was carried out in the Loei study area to determine the magnetic susceptibility level for each rock type. Rock outcrops were chosen from the existing geologic map to ensure that almost all rock units were sampled. The locations of rock samples are shown in Fig. 6.24. Each rock sample was cut as cube shape (1"x 1" x 1") and measured the magnetic susceptibility and density. The detail of sample locations, rock types, magnetic susceptibilities (SI unit) and densities were shown in Appendix II.

Most magnetic susceptibilities in the Loei area were conformed to the magnetic susceptibilities from the other rock samples reported by Clark (1997) as shown in Fig 6.25. In general, the magnetic susceptibilities of the Loei rocks conform fairly well to those in the fundamental theory (see Drobrin, 1985, and Telford et al., 1986). Basically, the magnetic susceptibilities higher than the more felsic rocks, and the felsic rocks have values higher than the sedimentary rocks. However, the magnetic susceptibility of rock samples depend largely on the magnetite contents in rocks, the samples in this study were mostly collected at the surface outcrops, so magnetite contents in the rock samples may be lost by weathering process.

6.2.6.1 Induced and remanent magnetization

Magnetized matter contains a distribution of microscopic magnetic moments. Unpaired electron spins are the most important source of magnetic moment. Magnetisation J is defined as the magnetic dipole moment per unit volume of material.

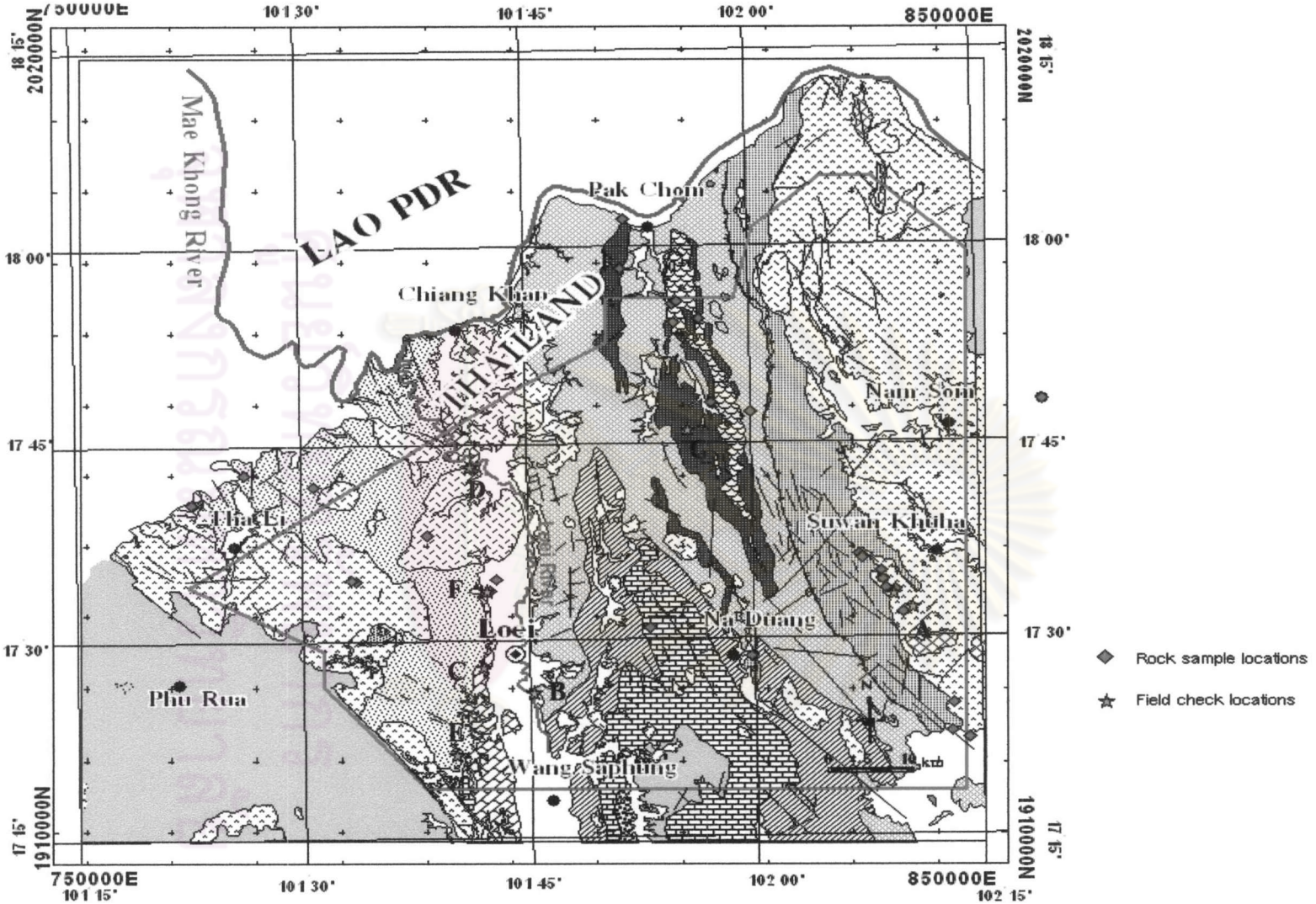

Figure 6.24 Location of rock samples and field check area plotting in the geological map (MRDP, 1988 and Chairangsee el al., 1990).

Induce magnetization (J_I) is the component of magnetization produced in response to an applied field. The induced magnetization varies with change in the applied field and vanishes when the field removed. Remanent magnetization or remanence (J_R) is the 'permanent' magnetization that remains when the applied field is removed and is essential unaffected by weak fields. The total magnetization is the vector sum of the induced and remanent magnetization:

$$J=J_I+J_R$$

For sufficiently weak fields, the induce magnetization is approximately proportional to the applied field. The constant of proportionality is known as the susceptibility (k). Thus if the applied field is F, the induced and the total magnetization are given by:

$$J=kF;\ J=kF+J_R$$

The Koenigsberger ratio (Q) is a convenient parameter for expressing the relative importance of remanent and induced magnetization. It is given by:

$$Q=J_R/J_I=J_R/kF$$

Thus Q>1 indicates that remanence dominates induces magnetization, where Q<1 implies that induced magnetization is dominant.

Fig. 6.25 plots observed susceptibility ranges and common susceptibility rages for various rock types and Fig. 6.26 shows ranges of Koenigsberger ratio found for a variety of rock types. .

From Fig. 6.26, many rocks in study area have no remanence, only induced magnetization, due to slow cooling deep in crust. They are granite intrusion, gabbo, and may be serpentinite. Rocks that do have remanent magnetization in the study area would be basalt lava flow, rhyolite lava flow, very high-level granite intrusion, and may be serpentinite body depended on depth of serpentinization.

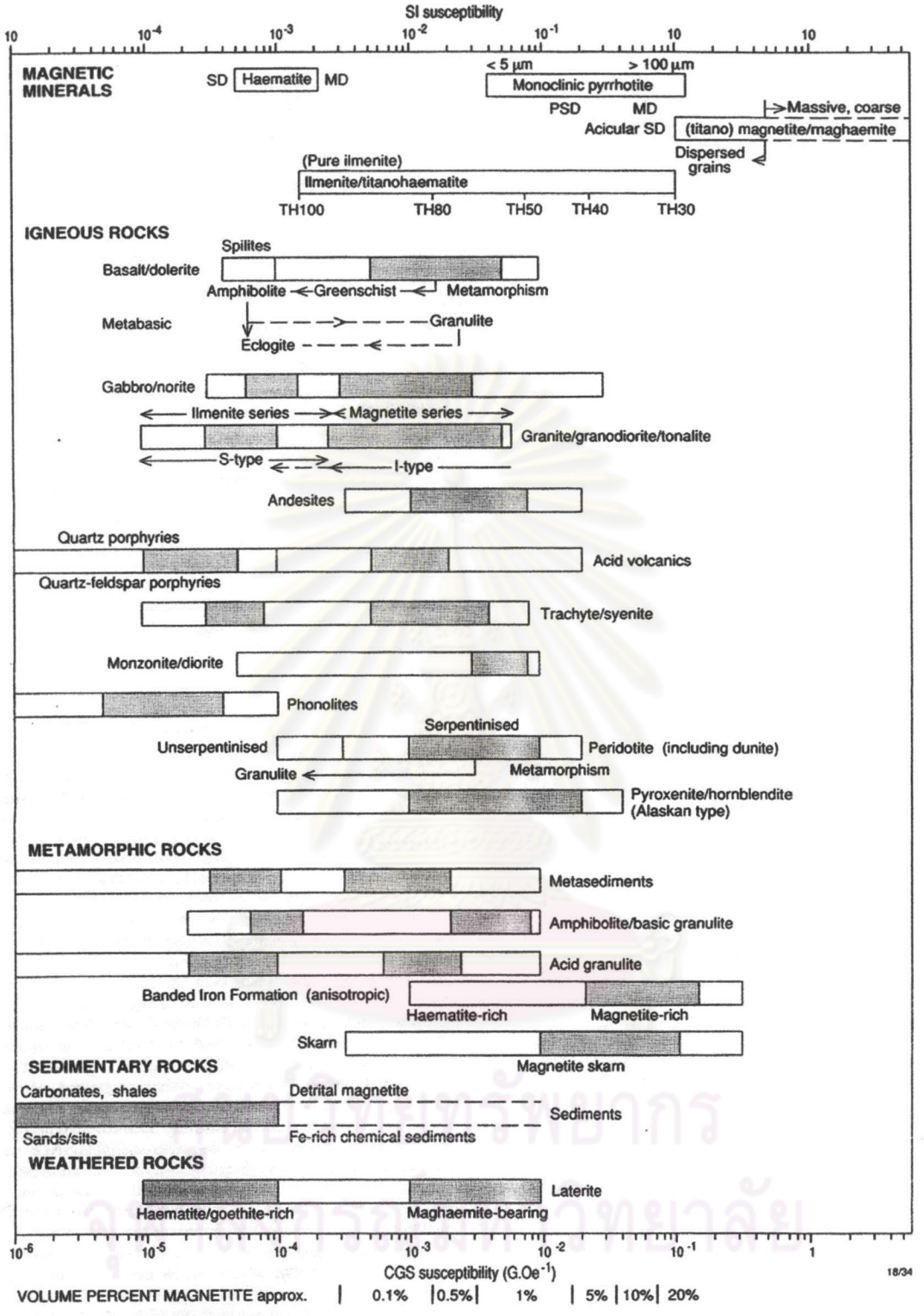

Figure 6.25 Observed and common susceptibility ranges of various minerals and rock types (Clark,1997).

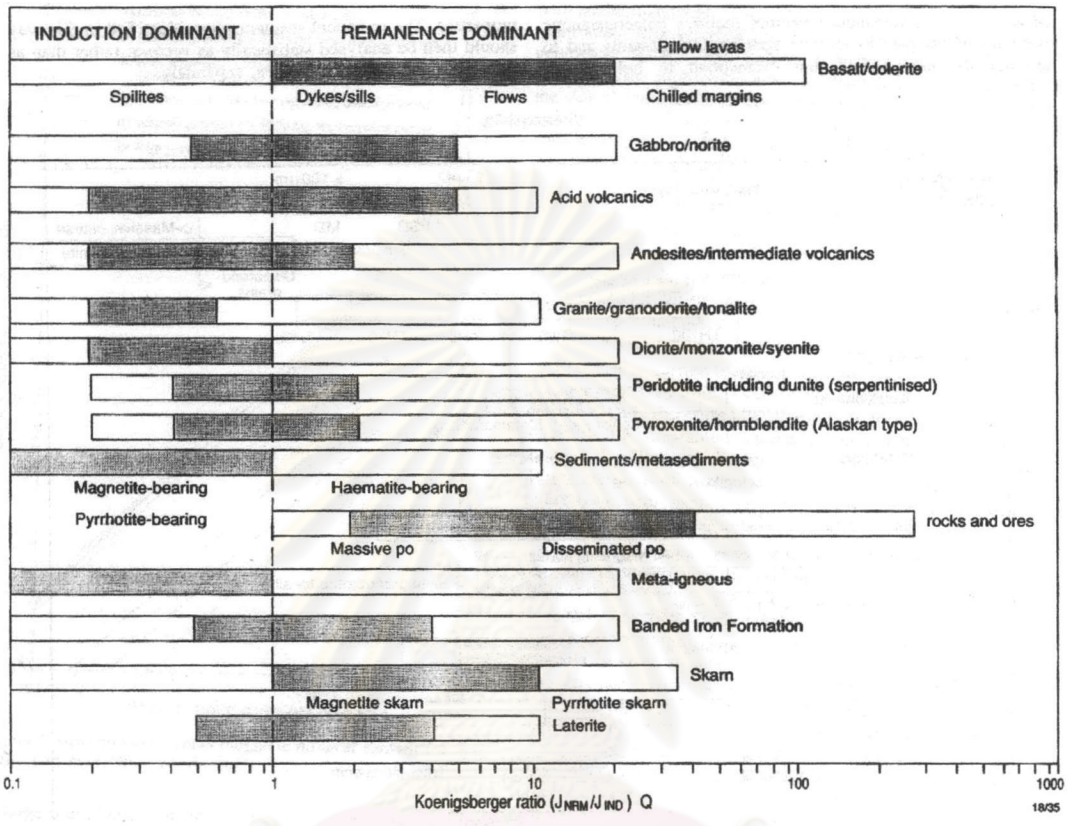

Figure 6.26 Observed and common ranges for Koeningsberger ratios of various rock types (Clark, 1997).

ศูนย์วิทยทรัพยากร
จุฬาลงกรณ์มหาวิทยาลัย

For the modeling, the high magnetic body of granite and ultra mafic zone along fault zone (Loei Suture Zone) are applied for 3D modeling. Therefore, they are assumed only induce magnetization. They also no exited rock sample taken to carry out remanence, and would have had to collect over 100 samples to det a good representation due to tectonic classification.

6.3 Geophysical interpretation

From the results of enhanced aeromagnetic maps, we were able to distinguish the magnetic responses due to the difference in magnetic susceptibilities, structures and deformations of the rock units in the area. Characterizing geophysical domains relies heavily on anomaly indicative of the rock units both of local surface and subsurface rocks. However, variable source depths within a domain may also contribute significantly to changes in anomaly shapes and sizes.

6.3.1 Magnetic domains

Based on the results from several enhanced image maps, we created a new interpretation map as shown in Fig. 6.27. With such integration and interpretation, the Loei study area is subdivided into three major magnetic domains on the bases of the magnetic intensities and features, namely eastern, central, and western domains. In general, boundaries of the individual domains coincide with the abrupt changes in average magnetic intensities, anomaly variabilities and orientations. Each domain was subdivided into sub-domains on the bases of local magnetization, surface and subsurface geology, lineament patterns and circular features described in the previous section. The characteristics of individual sub-domains are described by comparing with geological features (see Fig. 2.3).

6.3.1.1 Eastern domain

The eastern domain is the geophysical domain clearly trending in the almost north-south direction. The sharp boundary between the eastern and central domains is

regarded as the shear zone. This domain is chiefly composed of moderate to high magnetic intensities of volcanic rocks. The very high magnetic intensity unit in the southwestern part is indicated by ultramafic rocks. This rock unit is not shown in the geological map (Fig. 2.3). We subdivided the eastern domain into four main sub-domains (E1, E2, E3 and E4 sub-domains) based on the average magnetization and structural styles and patterns.

The E1 sub-domain shows the highest magnetic intensities and is located in the southwestern to southern parts of the domain, west of the Suwan Khuha district. Our field investigation and recently petrographical studies (Seusutthiya and Maopeth, 2001) indicate the occurrences of ultramafic rocks. These serpentinized rocks account for nearly 70 percent of the E1 sub-domain and mostly they align in the northwest-southeast trend. Shear zones are the main deformation structures, commonly exceeding 40 km in length and lying in the north-south direction. The shear zones are characterized by overlapping lineaments and form the 'S' shaped curvi-lineaments. Structural geophysical trends within the ultramafic rocks are largely aligned in the north and northwest trends. In addition, folds of variably magnetized strata are shown curved and banded magnetic patterns (Airo and Ruotoistenmark, 2000) are observed in the southern part. A series of synclines and anticlines with the average length of 10 km has the average axial plane in the north -south direction. Two north-trending strike-slip faults are also recognized in the northern part of the E1 sub-domain.

The E2 sub-domain is located in the northern half of the domain between Nam Som district and the Mae Khong river. This sub-domain is characterized by low to moderate magnetization corresponding to the felsic volcanic rocks (rhyolite and rhyolitic tuff) and granite plutons mapped by Chairangsee et al., (1990). This sub-domain can be distinguished from the E1 sub-domain by a sheared contact at depth, and a series of ultramafic rocks are served as an apparent contact of the boundaries between E1 and E2 sub-domains. To the southeastern boundary, the E2 sub-domain is connected with the E4 sub-domain by a series of ultramafic rocks.

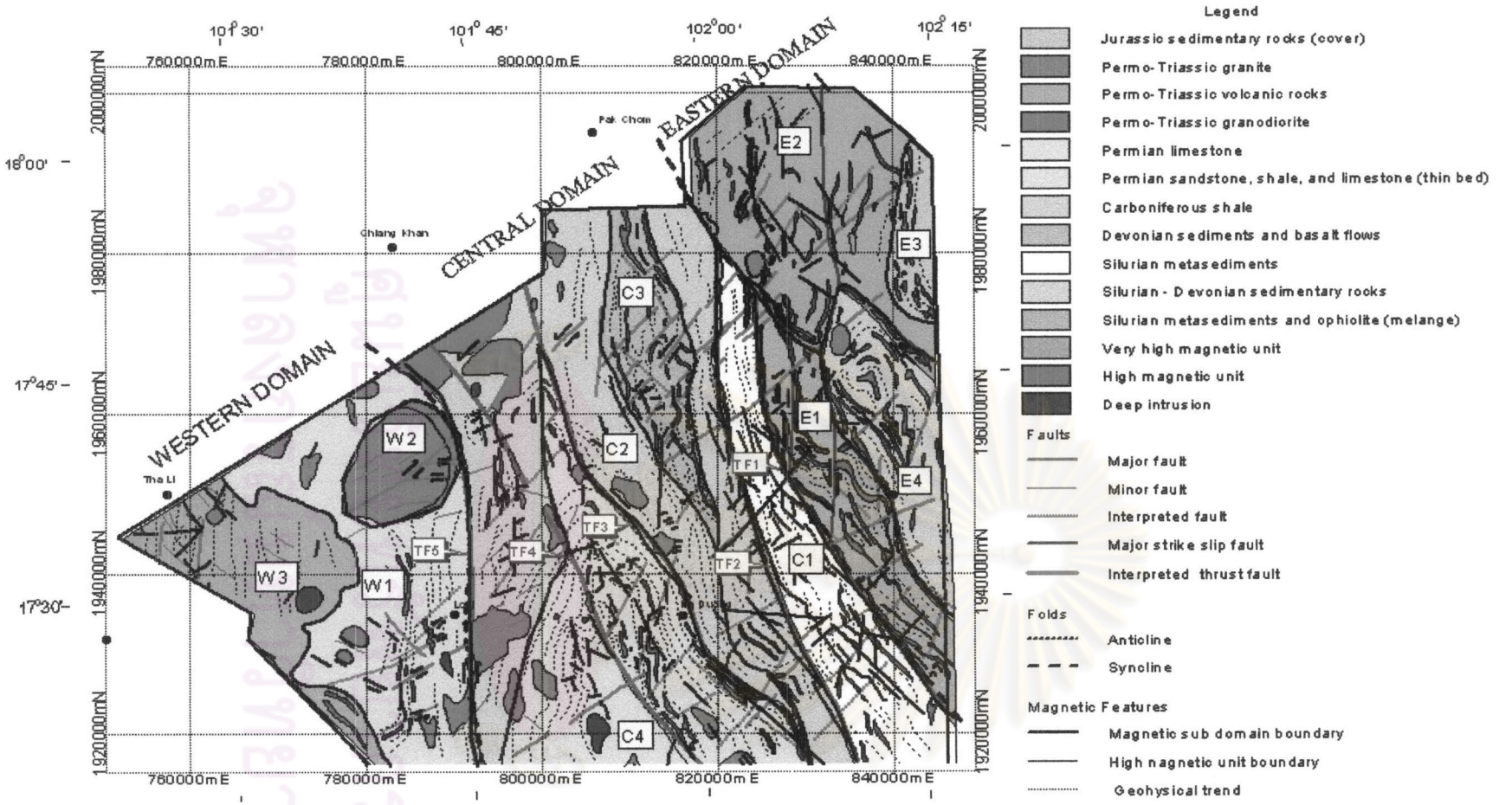

Figure 6.27 Geophysical interpretation map showing magnetic domain and major geological structures in the Loei study area.

The E3 sub-domain is located in the northeastern part of the domain to the east of the E2 sub-domain. This sub-domain is dominated by the large circular feature of the high magnetic unit (see Fig.6.3) with the north-trending linear structural trend. In the geological map, this sub-domain is mapped as Late Mesozoic non-marine sedimentary rocks of the Khorat group, which theoretically poses relatively low magnetization. The contrast in the magnetic responses lead us to believe that there are some felsic to intermediate intrusives underneath these overlain non-marine strata.

The E4 sub-domain is located in the eastern and central parts of the domain, between Nam Som and Suwan Khuha. This sub-domain displays moderate magnetic intensities. They are interpreted to represent sedimentary rocks underlying the felsic volcanic rocks of E2 sub-domain. A syncline as indicated by high magnetic unit, has the length of about 10 km and their axial trace almost in the north-south direction. The E4 sub-domain is separated from the E2 sub-domain by the strike-slip fault.

6.3.1.2 Central domain

The central domain is composed largely of low magnetic intensities. It can be subdivided into four sub-domains (C1, C2, C3 and C4 sub-domains) based upon magnetic shape, magnetic pattern, magnetic intensities and distribution of small high magnetic stocks.

The C1 sub-domain is the long, north- to northwest-trending low magnetic zone and corresponds to the rocks mapped as thick meta-sedimentary (phyllite and quartzite) strata (Chairangsee et al., 1990, MRDP, 1988) with mostly the northwest strike. The phyllite and quartzite were obviously affected by tectonic deformation and metamorphism much more intensely than all other rocks in the Loei area. The second oldest sedimentary rocks of Ban Nong Formation with the paleontological age of Silurian-Devonian by using the evidence of several corals such as *Heliolites sp*, H. barrandei (Sakagami and Nakornsri, 1987) and *Favosite sp* (Fontain et al., 1981). Thus the metamorphic rocks were at least of middle Silurian in age (Chairangsee et al, 1990). This sub-domain shows several long north to northwest-trending magnetic linear patterns interpreted to indicate major faults almost parallel to a regional structure. These faults,

up to 30 km long, identified clearly by the AEM image data because the extent of poorly magnetized faults with similarly magnetized sedimentary rocks is difficult to determine from the processed aeromagnetic data. To the south of the sub-domain, a series of AEM zone occurs following the major fault trend.

To the west of the C1 sub-domain is the C2 sub-domain, which is dominated by the low magnetic pattern with lineaments similar in patterns and styles to those of the C1 sub-domain. In the western part of this sub-domain, particularly north of Na Duang, circular highs magnetic presumably indicate intrusion stocks. This sub-domain was mapped as Carboniferous clastic sequences of the Wang Saphung Formation (Chairangsee et al., 1990). The circular magnetic anomalies observed in the central part were mapped as the felsic intrusive bodies (Chairangsee et al., 1990). As shown in Fig.6.9, the boundary between C1 and C2 sub-domains is indicated by the major thrust fault whereas to the west, the north-trending anticline is dominant.

Embedded into the C2 sub-domain in the roughly north-south direction is the C3 sub-domain, which consists of an elongate high magnetic intensity. This sub-domain is, more or less, equivalent to the mafic volcanic belt of basalt to basaltic andesite in composition (Chairangsee et al., 1990). This high magnetic unit shows many short northeast-trending lineaments with a series of folds in the same trend and two small thrust faults in the north-south direction.

The C4 sub-domain is mainly composed of low magnetic intensities. This sub-domain corresponds to thick Permian carbonates and clastic sequences of the Loei Group (Assavapatchara et al., 2001). A symmetrical variation of magnetic field intensity (Airo and Ruotoistenmark, 2000) shows a clearly defined lineament trend (see Fig.6.10) as a curved shape interpreted to represent the large folded structure with a long regional wavelength (Bunopas, 1992). The regional axial plane is in the northwest trend. The boundary between the C2 and C4 sub-domains is represented by the thrust faults in the northwest and northeast directions.

6.3.1.3 Western domain

The western domain is essentially composed of moderate magnetization. This domain was subdivided to three sub-domains (W1, W2 and W3 sub-domains) based on high magnetic patterns and intensities. The boundary between the central and western domains is indicated by the thrust fault in north-south direction.

The W1 sub-domain is indicated by moderate magnetization corresponding to the Permian sandstone strata with limestone interbedded (Chairangsee et al., 1990). This sub-domain shows the structural trend in the north-south direction similar to that of the regional mapped unit.

The W2 sub-domain is enclosed by the W1 sub-domain and shows a large circular feature with high magnetic pattern. This sub-domain is characterized by the northeast-trending major fault.

The W3 sub-domain is located in the western part of the western domain. It consists of moderate to high magnetization with the straight linear pattern in the north-south direction. This sub-domain corresponds with the Permo-Triassic felsic to mafic volcanic rocks of mainly andesitic composition (MRDP, 1988). There are a few small circular features, possibly suggesting volcanic vents occurring in the eastern and western parts.

6.3.2 Magnetic structures

Figs. 6.27 and 6.28 display lineaments of various patterns and styles have drawn using the image manipulation Arcview software. The lineaments were interpreted from visual hard copy images at scale 1:100,000 on the enhanced airborne geophysical data. Geologic lineaments were superimposed afterward as a separate layer. Comparison of the magnetic lineaments with the geologic lineaments shows that many of the magnetic anomaly trends coincide very well with geologic contacts or inferred faults.

The eastern domain is characterized by a rather irregular pattern of magnetic anomalies containing the long segments with the predominant north-south linear trend. This belt was donated by the sharp, long, northwest-southeast lineaments conformable with regional structures. These lineaments show the strike-slip fault motion indicated by the displaced lineaments and some lineaments were interpreted as shear zone by high magnetic units with the 'S' shaped features (Fig 6.28 (D)). The magnetic data also show the small folds consisting of several discontinuous, dextrally side-stepping lineaments and several tight folds are recognized in some locations. The structural pattern of this belt supported that the major structures was formed in response to a strong tectonic activity in the region. Moreover, the magnetic lineaments can be inferred as axial planes of the unmapped folds. Good examples are those in the E4 sub-domain with north-trending and northeast-trends.

The central domain comprises sets of the northeast-trending structural patterns. The prominent features are characterized by large-scale, open and upright folds dominated in both of the northern (C2 sub-domain) and southern (C4 sub-domain) parts, which are obvious in both magnetic and geologic maps. In the northern part of C3 sub-domain, the steeply-dipping and tightly-folded sedimentary strata are mapped within the area with high magnetic intensities. This zone forms a rather strong lineament pattern along most of its length and cross-cut the set of folds (Fig. 6.28(B)). In the southern part, the dominant northeast-trending lineaments are clearly visible and form large fold structures.

The boundary between the central and eastern domains is geologically mapped as the thrust fault (MRDP, 1987). In the geological map, the thrust marks the boundary between the metamorphic rocks and sedimentary strata of different ages. On the contrary, from this study, no signature shows the magnetic contrast between the western and eastern sides of this thrust fault boundary. From the processed aeromagnetic interpretation, a consistent sharp and strong magnetic gradient are only observed at the boundary between eastern and central domains which is far from the thrust fault in geological map about 5 km to the eastern side. However, from the AEM data (see Fig.6.12), the long lineament patterns of the high conductor at the same location suggest the thrust fault as shown in Fig 6.27.

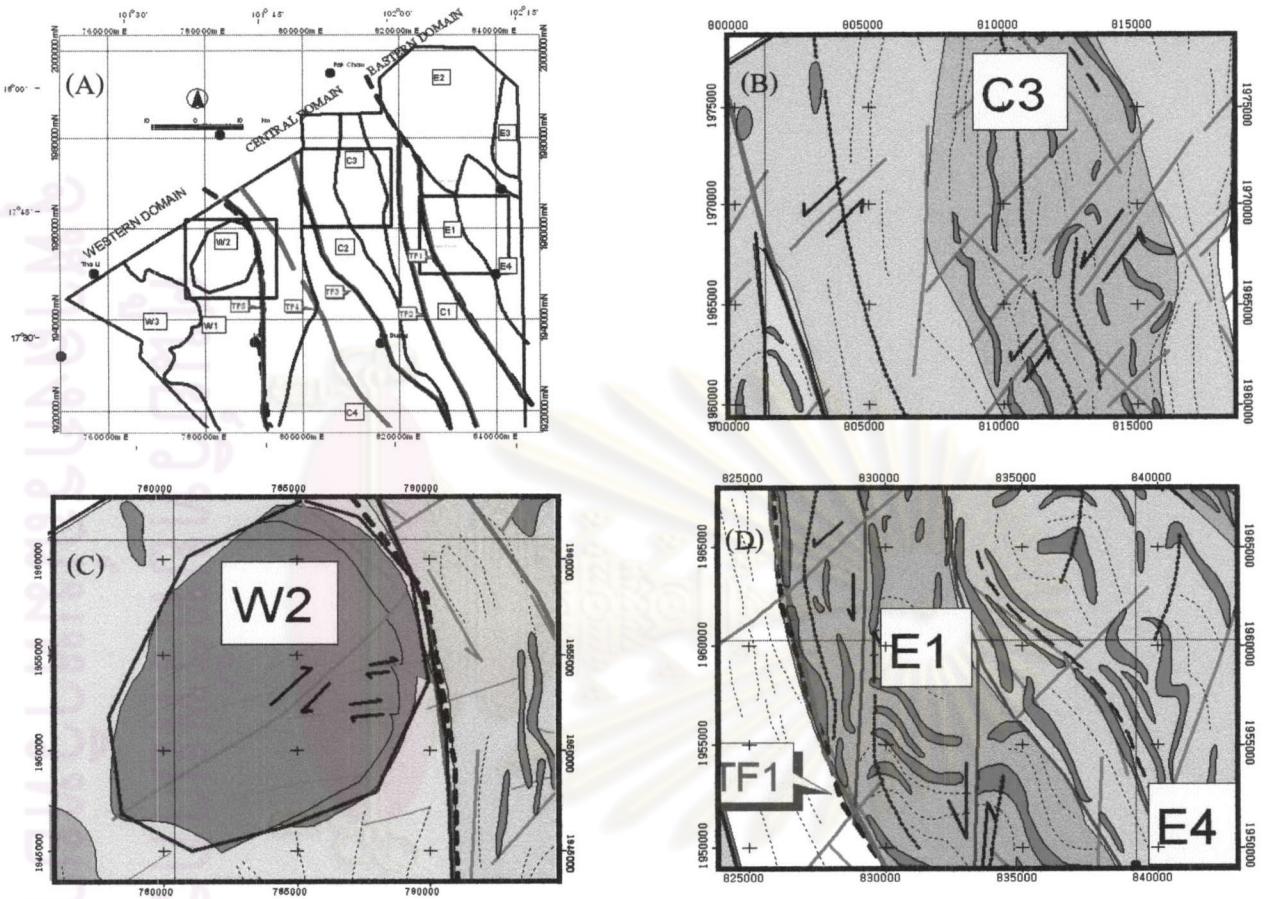

Figure 6.28 Detailed maps based on geophysical interpretation map showing major geophysical domain and their sun-domain (A), NE strike slip faults with left-lateral sense of movement in C3 (B), high circular magnetic units in W2 crosscut by the NE-trending right lateral fault (C), and major Sinistral north-trending strike slip faults in high magnetic unit in E1, and axial surface (D).

To identify a thrust fault by using geophysical data, in general, seismic and gravity data were commonly used for observing fault dippings. However, thrust fault can be identified by using tectonic setting and geological structures. Fluijm and Marshake (1997) described that the fault systems were common along the margins of convergent plate tectonic and along the margins of collisional origins, and faults tend to compose relay or parallel arrays. In addition, Airo and Ruotoistenmark (2000) discussed that thrust faults were typical geological boundaries, which separated regions or geological blocks showing different deformation styles and structures. In this study, thrusting which follows the main deformation stage was recognized as abrupt termination of one deformation style with regard to the adjacent one. Moreover, folding regions of higher or lower overall magnetic field intensity were often separated by series of large-scale fault zones or thrust faults parallel to the axial-plane strike or groups of smaller faults with the same trend. Therefore, in this study the thrust faults were interpreted based on the significance of magnetic patterns and geological features that are follow regional tectonic and structures.

Fig. 6.27 shows five thrust faults (TF1, TF2, TF3, TF4, and TF5) interpreted based on the processed aeromagnetic and electromagnetic maps. These faults mostly oriented in the roughly north-to northeast trends. All of them have the high to moderately dipping angle to the east. These faults range in length from 40 to 60 km. The TF1 with the total length of 50 km is located to the eastern most faults and demarcated between the eastern domain and the central domain. The TF 5 is located in the western most part and is a curvilinear fault. It serves as a boundary fault between the central domain and the western domain. The TF2 is the other thrust fault located to the east of the central domain and conforming with the geological map (MRDP, 1987, Chairangsee et al., 1990). The TF3 is located in the middle part of the central domain and separates a series of small tight anticlinal structures in the eastern side (C2 and C3 sub-domains) and a large open syncline fold in the west (C4 sub-domain). The TF4 (50 km long) is a thrust faults separated a large open fold in C4 sub-domain, which is parallel to the axial-plane strike and developed during fold.

The small northeast-trending lineaments are dominated in the western domain with the geophysical trend in the north-south direction. In Figs. 6.9 and 6.10, the boundary between central and western domains is indicated by contrasting magnetic patterns. The prominent structure of this domain is a large circular feature, which is mapped as a granite intrusion. Additionally, this circular structure was cross-cut by the northeast-trending lineaments probably indicated that the northeast lineaments are younger age than the granite intrusion (Fig. 6.28 (C)).

6.4 Magnetic modeling

From the magnetic data interpretation, we are able to construct the geophysical modelling by the assistance of the ModelVison software for both forward and inversion methods. As shown in the previous section, data from the RTP enhancement seems to give the best result. Therefore, magnetic response profiles of the RTP were selected for modeling. To simplify the line profile, cross sections were draw based on latitudes of study area (Fig. 6.29).

In this study, magnetic modeling is assuming only induce magnetization and using the magnetic susceptibilities measured from the rock samples in the Loei area as shown in the appendix II. The cross-section for modeling is in east-west direction because the main geological structure in the study area is in north-south direction.

Fig. 6.29 shows profiles of RTP aeromagnetic data along the east-west surveyed line with some data interpretation. Three cross-sections along line nos. L1970000N, L1950000N and L1920000N are selected for interpretation (Fig. 6.30). In the western side of the study area (at 790000E-800000E, M1), interpreted bodies have magnetic intensity higher than those of the surrounding areas, suggesting igneous bodies or dikes of possibly granitic composition. The circular feature (M2) in the western domain is the largest body and dips to the eastern side. On the surveyed line L1970000N at the 815000E (B1, B2), small bodies indicate high magnetic intensities of dikes,

corresponding to the volcanic (basalt) unit (C3) of the central domain. Additionally, D1, D2, D3, D4, D5 and D6 are corresponded to granitic dikes in central domain. Quite interesting are those at U1, U2, U3 and U4 between 830000E-835000E along the lines 1950000N and 1970000N. The series of high narrow magnetic dikes are encountered, and interpreted to indicate the east-dipping faults whereas the west-dipping dike corresponds to the mapped ultramafic rocks. These interesting anomalies are interpreted as the fault zone (TF1) in northwest -southeast direction, which borders of ultramafic and meta-sedimentary rocks (ophiolite zone) in the eastern domain (E1).

To make a scenario clearer, a perspective view in 3 D is displayed in Fig. 6.31 in an azimuth and inclination at 335° and 10°, respectively. The model is a result of the overlaying maps of the RTP grid at the top surface and upward 1000 meter at the bottom. The model shows that magnetic bodies continue to the deeper zone.

A crucial limitation of 3D interpretation of magnetic survey arises from the fundamental non-uniqueness of potential field source distributions. This ambiguity in source geometry can only be addressed by constraining models. The most important control on the reliability of magnetic models is information on magnetic properties. Understanding of the factors that determine magnetization intensities and direction for the geological units within the survey area is essential for resolving geological ambiguity in order to produce a reliable interpretation of subsurface geology.

ศูนย์วิทยทรัพยากร
จุฬาลงกรณ์มหาวิทยาลัย

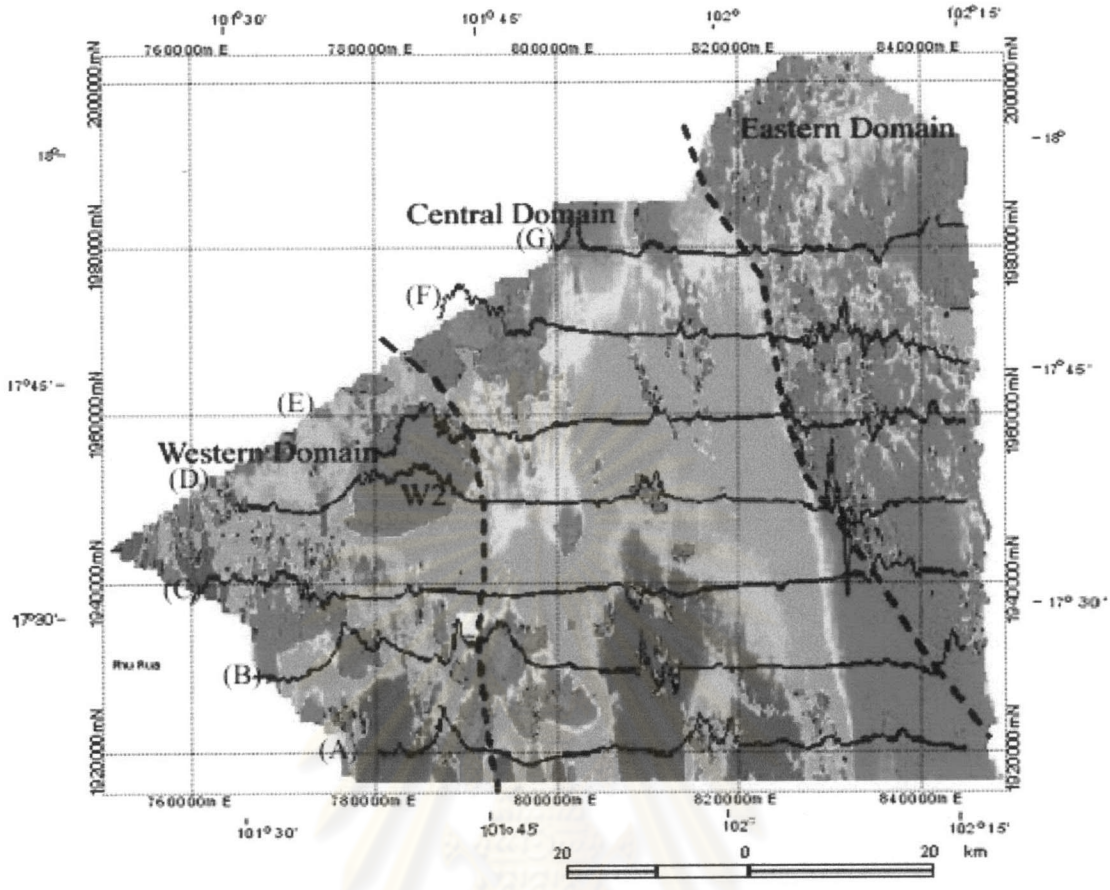

Figure 6.29 RTP aeromagnetic map of the Loei study area showing major magnetic domains and magnetic profiles at lattitudes (A) at 1,920,000N, (B) 1,930,000 N, (C) 1,940,000 N, (D) 1,9500,00N, (E) 1,960,000 N, (F) 1,970,000N and (G) 1,980,000 N.

ศูนย์วิทยทรัพยากร
จุฬาลงกรณ์มหาวิทยาลัย

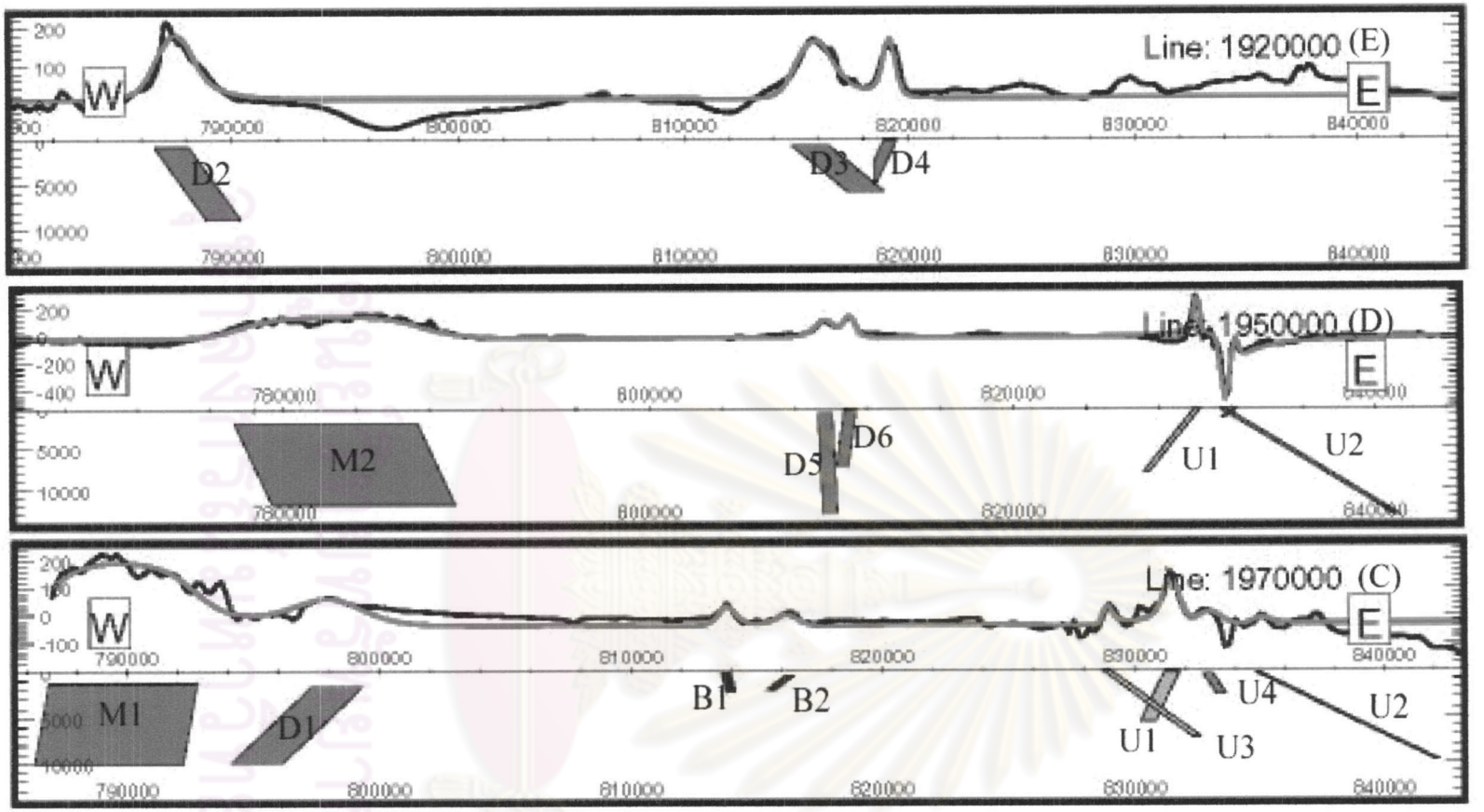

Figure 6.30 Magnetic model as interpreted from lines C, D and E in Fig.6.27. Note that M1, M2, B1,B2, D1,D2,D3 ,D4, D5, U1,U2,U3 and U4 bodies indicate high magnetic anomalous zones.

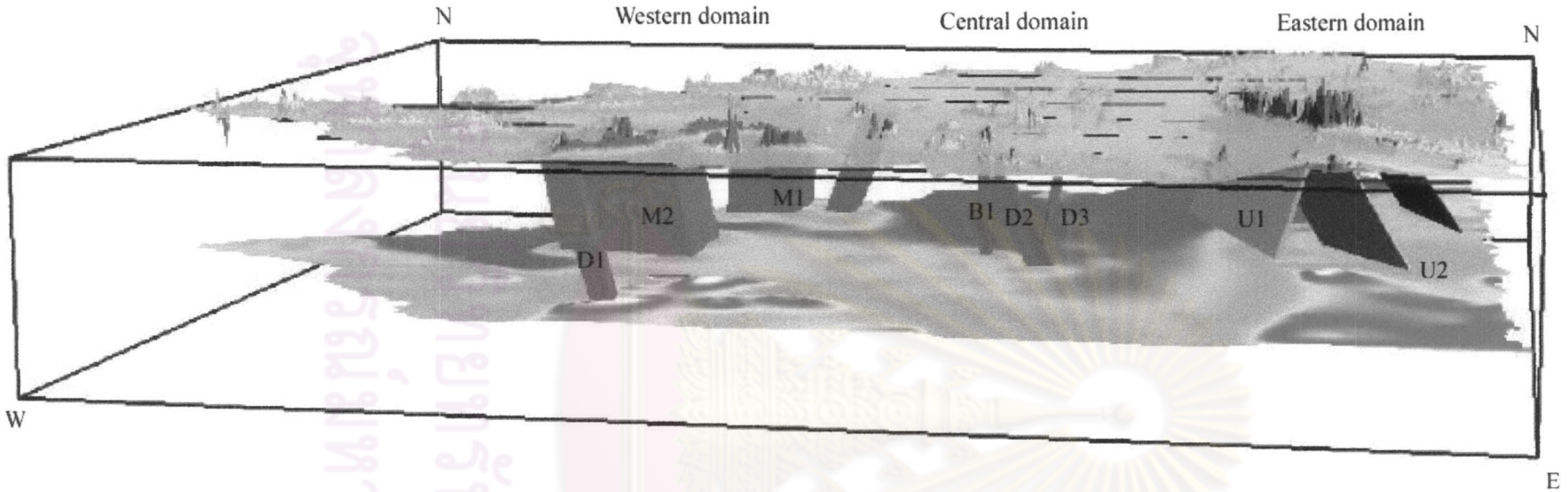

Figure 6.31 Perspective view of the Loei study area showing magnetic model in the dimension corresponding to the models illustrated in Fig. 6.30.

115

6.5 Field verification

In order to confirm the accuracy of the interpreted maps presented in the previous section, it is important to undertake field investigation in the selected areas where accessibility is not too difficult. Some high magnetic anomalies and structures from 8 sites as shown in Fig.6.24 were selected for more detailed field verification during the summer period of 2003.

Site A (Fig.6.32) is located in Ban Bun Tan, Suwan Khuha district and in the southern part of the E1 sub-domain with high magnetic anomaly. It is observed and interpreted that essential rocks of site A are ultramafic igneous rocks which occur within the areas earlier mapped by Chairangsee et al. (1990) as Silurian-Devonian meta-sedimentary rocks of the Namo Formation in the eastern part and Permo-Triassic volcanic and volcanic clastic rocks in the western part. The area mainly consists of deformed serpentinite rocks with anatomizing shear plane and 10^{o} striking foliation (Fig.6.32 A). Hydrothermal quartz veins and disseminated magnetite are observed in the rocks. Deformed serpentinized ultramafic rocks show degree of serpentinization with both ductile shear and shear fracture (Fig.6.32 B). Serpentinite outcrop with dark green color and sandstone lenses (Fig. 6.32 C) are found in the south of the road. To the east about 100 m from the serpentinite, the rocks are the deformed clastic sedimentary rocks, such as sandstone, shale, silicified rocks and chert (Fig. 6.32 D). Many shear planes and faults are in the north-south direction (mainly 170^{o} strike) and the east-west direction (mainly 70^{o} strike). The area is interpreted to represent partly of the dismembered or disrupted ophiolite complex. It is considered that this area is a main target area for future detailed exploration of Cr, Pt and talc deposits.

Field investigation shows that there are many kinds of igneous rocks and some meta-sedimentary rocks. Most of the igneous rocks are serpentinite and peridotite. Additionally, in some parts of the exposed rocks in site A area, such as hornblendite, gabbro and diabase, were also observed by Seusutthiya and Maopech (2001). The

meta-sedimentary rocks are mainly quartzite and phyllite. Chert or meta-chert in the area is massive beds with deformation structures. The association of ultramafic rocks and meta-sedimentary rocks occurring with in the fault zone as recognized by Landsat interpretation map lead to the conclusion that the rocks in this area occurred in the mélange zone. A more detailed lithological map of the field checking area is shown in Fig. 6.33. Moreover, geochemical data of the more mafic rocks reveal that the rocks were originated from the oceanic-crust environment (Daorerk et al., 2003).

Site B (Fig.6.34) is situated in the C2 sub-domain and is characterized by the bright spot of high magnetic anomaly (see 6.3) with the aerial extent of 1x1 km. The field evidence is supported by the appearance of magnetite skarn type deposits developed at the contact zone of silicified granodiorite (Figs. 6.34 A and B). A few of hornfels and granodiorite floats with some disseminated sulfides are interesting for sulfide Au skarn deposit area.

Site C (Fig. 6.35) in the C2 sub-domain is displayed by a zone of high magnetic anomaly (Fig. 6.3) and high K contents (Fig. 6.15). The site, therefore, represents the intermediate calc-alkaline intrusion with strong potassic alteration. Field investigation indicates that the main rock type is granodiorite with potassic and argillic alteration. The area is mainly covered by a highly weathered mudstone (Fig. 6.35 A) with quartz vein (20–cm wide in 10^{o} strike). In some part areas, silicified mudstone with highly shear are observed. Joints and foliations are in the northwest-southeast direction (320^{o}). Gossan floats and outcrops (Fig. 6.35 B) with silicified iron stains are found in the silicified shear zone, and highly weathered porphyry rocks. These features are interesting guides for sulfide and gold deposits.

Site D (Fig. 6.36) is located in the W2 sub-domain. It displays a high magnetic anomaly with the aerial extent of 1x1 km. The surveyed area shows granite intrusion in contact with sedimentary rocks such as limestone and meta- siltstone. Both endo-and exo-skarns are observed at the contact zone. Iron skarn mineralization occurs within the contact zone as shown by boulders of iron ores and in the abandoned open mine. Iron

(A)

(B)

จุฬาลงกรณ์มหาวิทยาลัย

Figure 6.32. Man-made exposures in the E1 sub-domain and site A (grid no. 834943E/1943409N) (Ban Bun Tan 1) showing

(A) serpentinite rocks with 1-thick under laterilitic soil, and

(B) close-up view of deformed serpentinized ultramafic rocks with anatomizing textures.

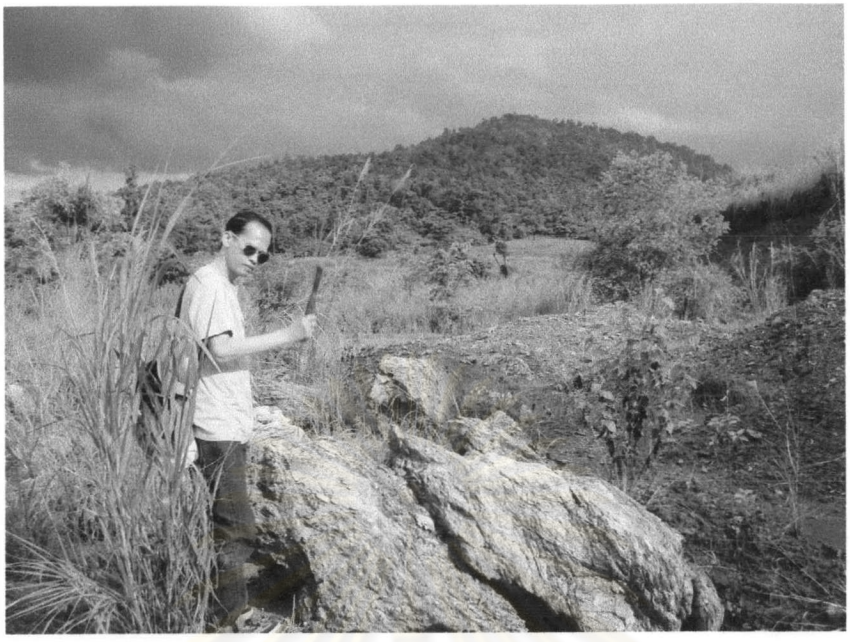

(C)

(D)

จุฬาลงกรณ์มหาวิทยาลัย

Figure 6.32 (cont.). Back hole-cut exposure at Ban Bun Tan 2 (grid no. 837128E/1941464 N) showing

(C) strongly deformed serpentinite body (2x1 m) with east-dipping plane of foliation (the author is to scale), and

(D) large of deformed and fractured clastic rocks.

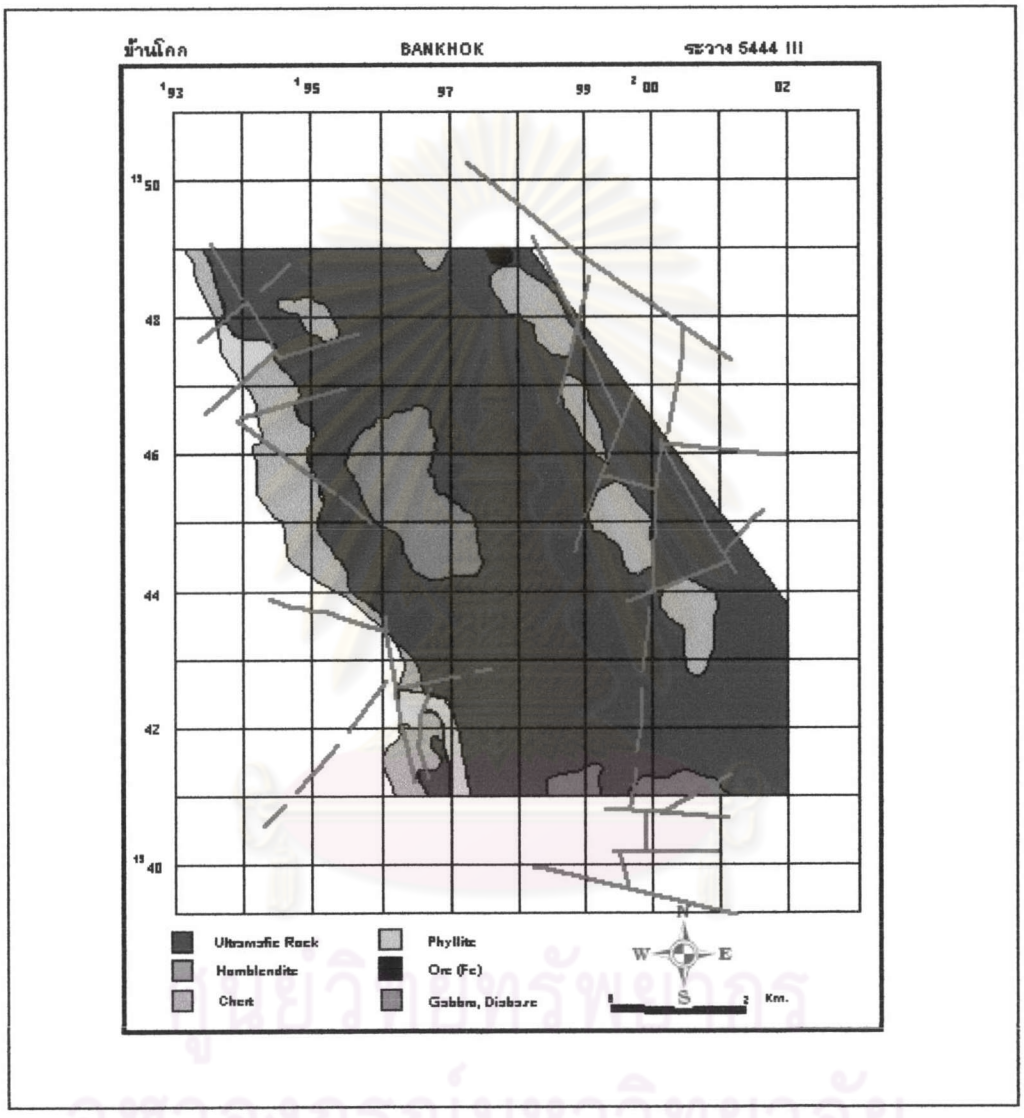

Figure 6. 33 Lithological map of Ban Bun Tan area, Suwan Khuha, Nong Bua Lumphu Province, showing distribution of rock types.

(A)

(B)

จุฬาลงกรณ์มหาวิทยาลัย

Figure 6.34 Natural granite exposures (grid no. 785630E/1933020N) in C2 sub-domain or site B of Fig.6.24 showing

(A) the natural exposure showing silicified granodiorite with high disseminated sulfide mineral (1-2%) along the valleys, and

(B) some of meta sediments nearby, such as the north-trending, steeply-dipping limestone.

(A)

(B)

จุฬาลงกรณ์มหาวิทยาลัย

Figure 6.35.Natural exposure of site C (grid no. 792475E/1929553N) in C2 sub-domain showing

(A) a highly weathering mudstone with quartz vein (20 cm), and

(B) expose quartz striking north with 70^{o} dipping to the east

(Dr. Jayson Meyers is to scale).

(A)

(B)

Figure 6.36. Man-made exposure of hornfel/skarn rocks with high magnetic anomaly within circular feature at Ban That located in the W2 sub-domain (grid no. 784976E/1961325N) showing

(A) general view of skarn rocks, and

(B) close-up view of westward dipping magnetite/hematite skarn.

minerals mainly specular hematite and few magnetite grains are found in veins striking in the north-south direction and dipping 50^{o}-60^{o} to the west (Fig.6.36 B). This area has high potentials for Fe and Au skarn deposits.

Site E (Fig. 6.37) is located right at the Thung Kham mine area of the W1 sub-domain. The area E is nearby the contact boundary between the C2 and the W1 sub-domains. The area is shown by high magnetic and EM anomalies. The field investigation reveals that the rocks in this area are mainly red to reddish brown-bedded siltstone (Fig. 37 A) with bedding 220^{o}strike, and 40^{o}dip. Some floats of limestone and granodiorite boulders are commonly observed. Breccia zone in siltstone with magnetite enriched veins and veinlets (Fig. 6.37 B) probably with gold mineralization (Yemned, 1999) in this area.

Area F (Fig.6.38) is located in the C2 sub-domain. Although in term of geophysical signal, no anomalies are recognized by both magnetic and radiometric surveys. However, the survey area is located between the central and the western domains, structure features in this area are quite essential. Field investigation shows a large quarry (20x50cm) (Fig.6.38 A). Fold axis (Fig.6.38 B) is clearly observed in the north-south direction, almost following the contact boundary fault between the C2 and the W1 sub-domains. Some faults and joints consists mainly 1-2 cm-thick shale and 10-15 cm silicified siltstone (or chert) beds with attitudes of $15^{o}40^{o}$ SE and $0^{o}60^{o}$ E, respectively.

Area G (Fig. 6.39) is situated in the C3 sub-domain where high magnetic anomalies are present. Based on the field investigation, it is observed that thin ribbon chert beds show recumbent fold with the fold axis in the north-south direction. Lateral faults and thrust faults are clearly observed almost parallel with the fold axis. The field investigation conforms very well with the interpreted surface and subsurface structures by airborne geophysical data.

(A)

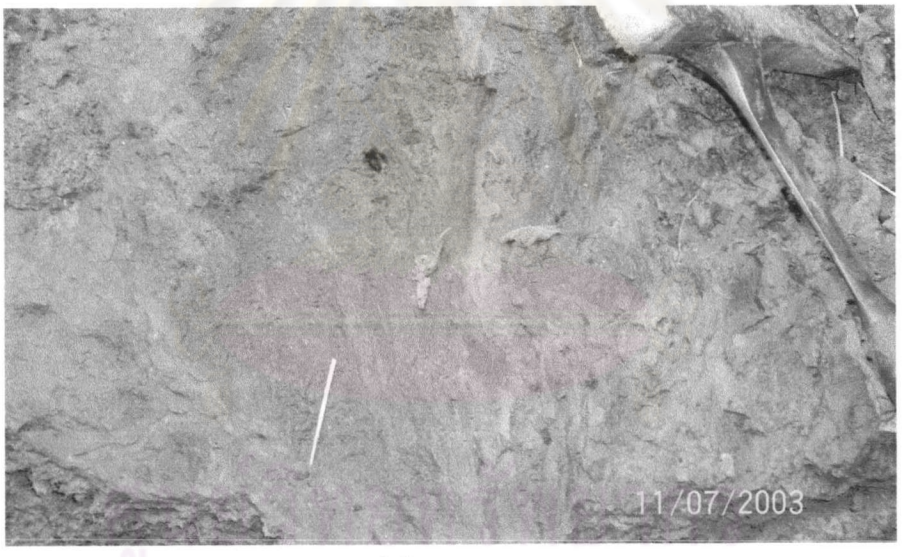

(B)

Figure 6.37. Artificial exposure of vein-filling fractures in fine-grained clastic rocks in the W1 sub-domain characterized by high magnetic and high EM anomalyies (grid no. 783520 E/ 1920800N) and within the Thung Kham mine area showing

(A) quartz-feldspar (mainly weathered to clay) veins and veinlets in the red silstone, and

(B) iron-rich veinlets in the red silstone.

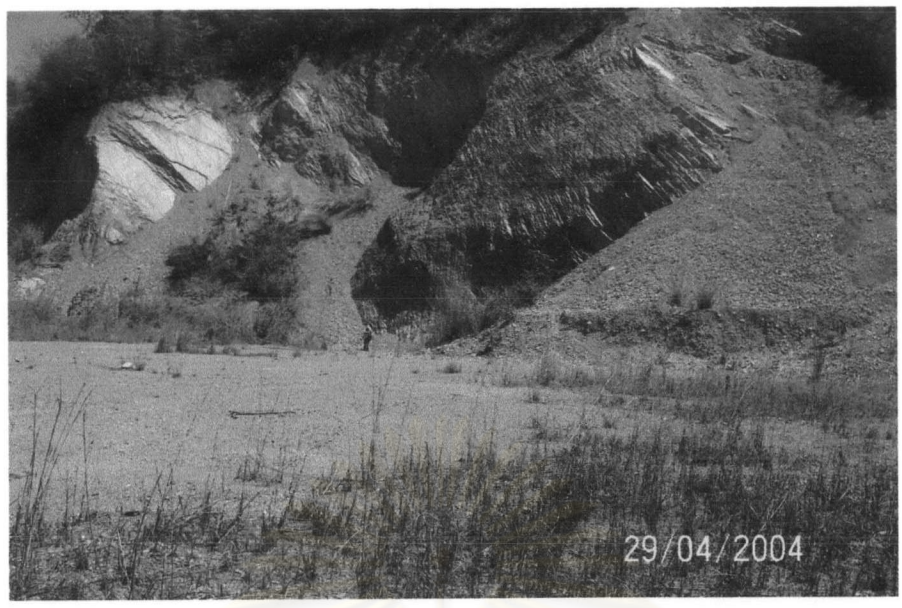

(A)

(B)

ศูนย์วิทยทรัพยากร
จุฬาลงกรณ์มหาวิทยาลัย

Figure 6.38. Bulldozer –cut exposures of folded shale and chert beds in the C2 sub-domain nearby the W1 sub-domain (grid no. 787016E/1943671N) showing

(A) interbedded shale and silicified siltstone with mostly high angle eastward, and

(B) open folded strata of shale and silstone with the fold axis almost in the north-south direction.

(A)

(B)

Figure 6.39. Man-made exposures of Devonian bedded "ribbon" cherts interbedded with thinly bedded tuffaceous silstone in C3 sub-domain (grid no. 810619E/1966760N) showing

(A) recumbent folded structure with axial planes of averaging north-trending strike and low angle (10^{o}-30^{o}) east dip, and

(B) close-up view showing chert beds with high resistance and tuffaceous siltstone beds with much lower resistance.